Peptide-Based Heme−Protein Models

Angela Lombardi,* Flavia Nastri, and Vincenzo Pavone

Department of Chemistry, University of Napoli "Federico II", Complesso Universitario Monte S. Angelo, Via Cynthia 45, I-80126 Napoli, Italy

Received March 14, 2001

Contents

I. Introduction

Metalloproteins are involved in fundamental biological processes and utilize a relatively small number of metal-based prosthetic groups to serve numerous and diverse chemical functions.[1,2] The heme−proteins family represents a fascinating example in this respect: a single prosthetic group, the heme, promotes a variety of functions, such as dioxygen storage and transport, electron transfer, hydroxylation and oxidation of organic substrates, and hydrogen peroxide disproportion.[3] How different proteins are able to fine-tune the environment of the heme cofactor, thus producing such different chemistries, is becoming increasingly clear through the study of natural and artificial model systems.

High-resolution X-ray crystallographic data as well NMR analysis available for an increasing number of heme−proteins, have deeply contributed to understanding their reactivity and structural and electronic properties at the molecular level.[4−16] It is now well ascertained that the protein matrix, which surrounds the heme active site, controls the intrinsic reactivity of the prosthetic group, selecting one reaction as the only or predominant one. The protein composition and structural organization of the peptide chain dictate the properties of the primary (metal coordination geometry, number, type, and donor properties of the axial ligands) and secondary (local dielectric constant, hydrophobicity, and hydrogen-bonding interactions near the active site coordination sphere) coordination shells. Further, the protein directs long-range interactions.[17] These factors all contribute to the functional specificity of the heme.[18−24]

Replacement of the fifth imidazole axial ligand in hemoglobin and myoglobin with a thiolate, as found in cytochrome P-450-dependent monooxygenases, causes the switch of the heme−protein function from reversible dioxygen binding to dioxygen activation.[25] In peroxidases and catalases, involved in hydrogen peroxide activation, the fifth axial ligand is generally a histidine and a tyrosine residue, respectively.[11] Finally, cytochromes *c* play a key role in electron transfer, and they are characterized by a histidine/methionine axial ligand combination and in particular by the covalent linkage between positions 7 and 12 of the heme with two cysteine residues of the protein chain.[13] Cytochromes *b*, which also participate in electron transfer, are instead characterized by *bis*-histidine axial coordination with an iron ion in the low-spin state.[16]

The local protein environment surrounding the heme more finely regulates the heme−protein properties, such as the iron redox potential.[26−31] For instance, a large number of positively charged residues around the heme in hemoglobin and myoglobin may favor a low oxidation state for the iron, making it ready to bind dioxygen. On the contrary, the progressive change in the polarity of the surrounding peptide environment, from a negative charge distribution in cytochromes *b* to a positive one in cytochromes *c*, determines a gradual increase in the Fe(III)/Fe(II) redox potential. The resulting stabilization of the matching Fe(II) and Fe(III) states enables cytochromes to mediate the electron transfer.

While the control of the functional specificity by the primary coordination sphere is well understood, the contribution of medium- and long-range interactions is still not completely rationalized, and their molecular description remains to be determined. Therefore, a large number of artificial model systems are being developed in an attempt to (i) provide further insights for structure−activity relationships, (ii) understand the minimal requirements for function, (iii) reproduce the properties of the parent

* To whom correspondence should be addressed. Phone: +39-081 674418. Fax: +39-081 674090. E-mail: lombardi@chemistry.unina.it.

10.1021/cr000055j CCC: $36.00
Published on Web 09/25/2001

Angela Lombardi is Professor of Inorganic Chemistry at the University "Federico II" of Napoli. She was born in Guardia Sanframondi (BN, Italy) and received her Ph.D. degree in Chemistry from the University of Napoli in 1986. She was a postdoctoral fellow and research associate in the group of Vincenzo Pavone at the same University. In 1990 she was a Visiting Fellow at NIH (Laboratory of Experimental Carcinogenesis, NCI), and in 1995 she joined William F. DeGrado's group, at the DuPont-Merck Pharmaceutical Co. Her research interests are mainly focused on the development of metalloprotein models as tools for understanding the action mechanism of metalloproteins and metalloenzymes, especially regarding the role played by metal ions in biological processes.

Flavia Nastri is a Research Associate at the University "Federico II" of Napoli. She was born in Napoli (Italy) and received her Ph.D. degree in Pharmaceutical Chemistry from the University of Napoli in 1990. She was a postdoctoral fellow in the group of Vincenzo Pavone at the same University. In 1994 she joined Daniel Mansuy's group at the Université René Descartes, Paris (France). Her research interests are centered on peptide and protein chemistry, covering the fields of synthesis and structural and functional characterization of biologically active peptides and metalloprotein models.

natural proteins in smaller molecules, and (iv) most importantly construct new, tailor-made molecules useful for biomedical, pharmaceutical, biological, and environmental applications.

A. Developing Heme–Protein Mimetics

Over the years a large number of low molecular weight heme−protein mimetics have been developed using quite different strategies. They differ in molecular structures, ranging from simple *meso*-substituted *tetra*-arylmetalloporphyrins to more complex peptide−porphyrin conjugates.[32] The chemical structures of porphyrins usually employed in model systems are illustrated in Figure 1.

A common feature in the compounds so far developed is the assembly, around the porphyrin ring, of several different chemical components, which are intended to fulfill the features of the protein matrix and make the heme ready to accomplish specific functions.

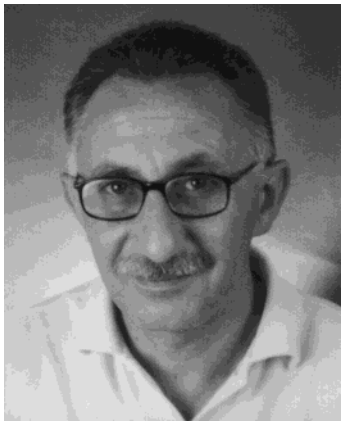

Vincenzo Pavone, 49 years old, is Professor of Inorganic and Bioinorganic Chemistry at the University "Federico II" of Napoli. He received his Ph.D. degree in Chemistry with Paolo Corradini from the University of Napoli (1976). He spent two years at NIH (1978–1980) in the Laboratory of Chemical Biology (NIAMDD) and six months (1987) at the Mitsubishi Kasei Institute of Life Science (Japan). He is a member of the Advisory Board of the Science and Technology Division of the University of Napoli. His scientific interests are focused on peptide/protein–metal ion interactions and include the design, synthesis, and structural characterization of "miniaturized metalloproteins".

As an example, to obtain oxygen carrier models, two main requirements are needed: (1) stabilization of a five-coordinate heme complex having an imidazole proximal ligand and (2) prevention from further oxidation of the iron−dioxygen complex.[33−36] In the natural systems these mandatory conditions for efficient reversible oxygen binding are accomplished by the presence of the steric bulkiness of the protein moiety, which blocks the formation of a μ-oxo bridge between two heme complexes and brings the axial ligand in the correct coordination position.

On the other hand, a chemical model system for the dioxygen activation, resembling the cytochrome-P450 catalytic cycle and efficiency, should embody the following features. (1) An axial thiolate ligand should be present, as it fundamentally contributes to the heterolytic cleavage of O−O bond and modulates the intrinsic reactivity of the high valent iron-oxo species. (2) A steric protection of the porphyrin ring is required to prevent the rapid degradation of the catalyst by the oxidizing species produced during the reaction. (3) Further, to control the chemio-, regio-, and stereoselectivity in oxygenation reactions, a chiral environment, able to selectively recognize a defined substrate, should be constructed around the heme group.[37−40]

Since the early 1970s, the development of low molecular weight heme−protein models was based on the construction around the heme of bulky moieties by covalently linking aromatic or aliphatic substituents to the porphyrin ring.[33−40] Although these model systems have gained considerable success as they deeply contributed to a better understanding, at a molecular level, of the properties of the natural heme−proteins, similar success has not been achieved with functionality, and therefore, they

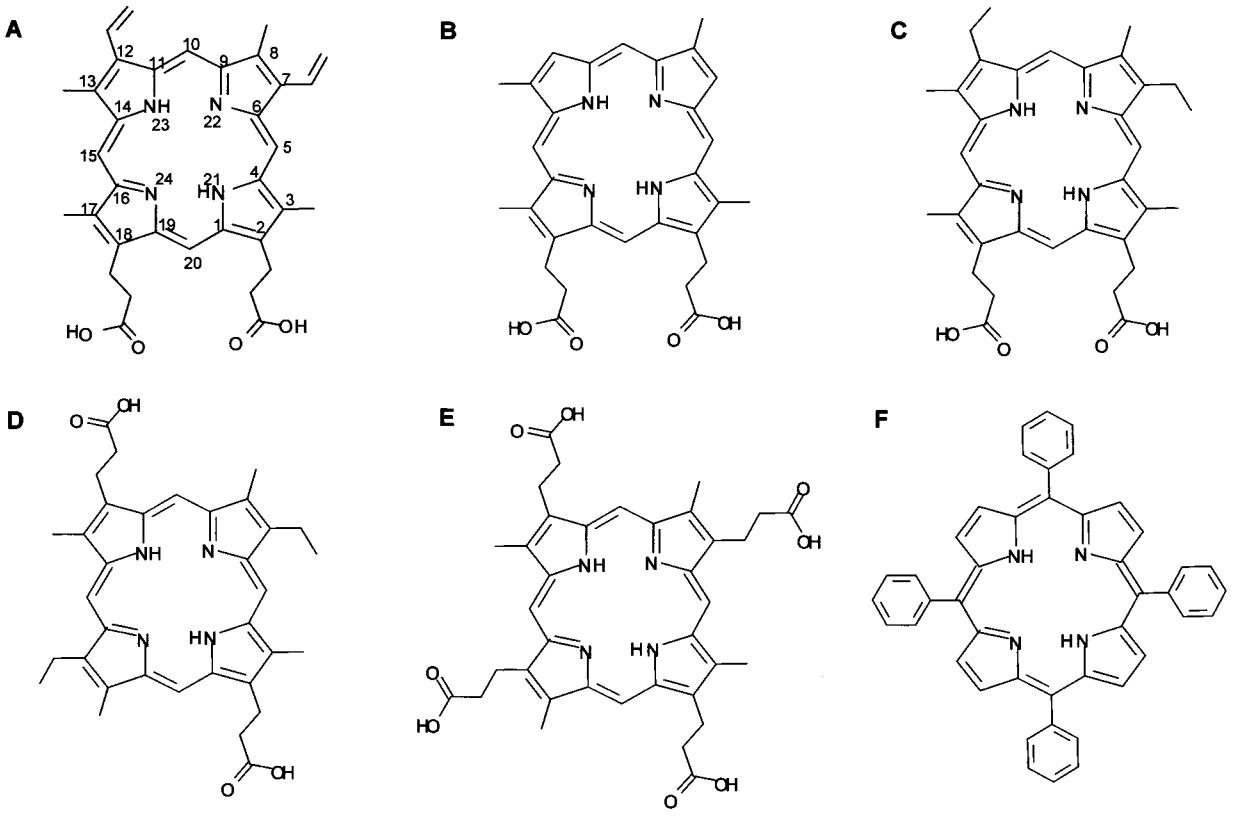

Figure 1. Chemical structures of porphyrin rings: (A) protoporphyrin IX; (B) deuteroporphyrin IX; (C) mesoporphyrin IX; (D) mesoporphyrin II; (E) coproporphyrin; (F) *meso*-tetraphenylporphyrin. The numbering scheme according to the IUPAC nomenclature is also reported in part A; commonly, the 5, 10, 15, and 20 positions have been also referred to as *meso*-positions.

have not yet found widespread practical applications. Several excellent review articles, which collect the main results in this area, have appeared in the literature.[35−43]

In more recent years, the field of heme−protein mimetics broadens to include more elaborate peptide-based models. In this review we will focus on these novel engineered models, mainly covering the literature from 1990 to date. The pioneering works on chelated hemes,[33,34] which were basic for the development of more elaborate systems, will also be briefly surveyed for completeness and clarity of discussion. However, for a more detailed description of these systems, the reader can refer to previous excellent reviews.[35−43]

Peptide-based models are having an enormous impact on our understanding of the factors governing the heme properties, as they seem to be better candidates to mimic both the structural characteristics and reactivity of the natural systems. Peptide architecture around the heme can serve for substrate recognition and to reproduce the efficient chemio-, regio-, and stereoselectivity of natural heme−proteins. Peptide models stand at the crossroads of small molecule models and large proteins. Their structures are simple and hence more easily understood than their natural counterparts. They simultaneously have sufficient size and chemical diversity to allow the construction of functional binding and catalytic sites.[44−49]

The development of peptide-based models takes advantage of recent progress in both the design and synthesis of peptides and proteins. It is now possible to construct rigid scaffolds able to accommodate substantial changes in their sequence without loosing their three-dimensional structure because the principles governing folding and stability of peptides and proteins are better understood and advanced tools for their design are available.[49−59] Hence, it is possible to build recognition and catalytic sites in a scaffold and to systematically vary the amino acid composition, thus allowing one to (1) optimize the structural and functional properties of the initial target, in terms of stability, catalytic activity and selectivity, (2) test how small changes in the sequence affect the properties of the heme and whether they are able to switch the heme function from one to another, and (3) investigate not only the effect of variation in the first coordination sphere but also the influence on the activity of medium- and long-range interactions. Peptide models offer the additional advantage of solubilizing the high hydrophobic heme in aqueous solution by simply accommodating the heme group in a hydrophobic pocket of an amphiphilic structure. Finally, the functional parameters can be improved with an iterative process of redesign and synthesis.

In this review two different types of peptide-based heme−protein models will be discussed: (1) models in which peptide chains are covalently linked to the heme and (2) models in which peptide chains incorporate one or more heme groups by noncovalent self-assembling around the heme. The use of the porphyrin ring as template for inducing helical conformation will also be described to highlight the ability of

porphyrin in directing peptide sequences into the desired fold.

We will summarize the different design approaches used in the construction of the examined models, which span from de novo design to the miniaturization process. The synthetic procedures applied will be also examined, especially regarding their innovation aspects. Finally, we will focus our attention on the structural and functional aspects that have been basic to structure−activity relationships.

B. Spectral Properties of Metalloporphyrins and Heme−Proteins

UV−vis spectroscopy has been widely applied for the characterization of peptide-based heme−protein models because it is one of the most powerful techniques for the analysis of the heme properties. Useful information on artificial porphyrin-containing systems can be obtained by comparing their spectral properties with those of natural heme−proteins and vice versa. This section will provide a brief survey of the main spectral features of metalloporphyrins and heme−proteins, which could be helpful to nonspecialists in understanding the subsequent sections. For a more detailed description of porphyrin and metalloporphyrin spectra together with the theoretical aspects of the spectral transitions, the readers can refer to many excellent reviews on the arguments.[60−63]

The porphyrins and their various metal complexes show very distinct spectra, and UV−vis spectroscopy can be conveniently applied to ascertain the insertion of the metal into the porphyrin ring, the oxidation and spin state of the metal, and the nature of the axial ligands. The highly conjugated π-electron system of the porphyrin ring is responsible for its intense color. Two $\pi \rightarrow \pi^*$ electronic transitions are responsible for the absorption bands, typically found in the porphyrin spectra.[60−63] An intense band (molar extinction coefficient $\approx 10^5$ M^{-1} cm^{-1}) is detected around 400 nm, and it is referred to as the *B* band, Soret band, or γ band; much weaker bands (molar extinction coefficient $\approx 10^4$ M^{-1} cm^{-1}) are observed in the 500−600 nm visible region. These weaker bands are referred to as *Q* bands or $\beta-\alpha$ bands. The α band corresponds to the lowest porphyrin $\pi \rightarrow \pi^*$ singlet transition Q_o and the β band to the vibronic envelope Q_v.[60,61]

The visible bands are very sensitive to the metal inserted into the porphyrin ring and to peripheral substituent groups. The Q_o and Q_v transitions are polarized in the *x*, *y* plane of the porphyrin; for a metal porphyrin with D_{4h} symmetry, the dipole transitions in the *x* and *y* directions are equivalent and both the Q_o and Q_v transitions are doubly degenerate. Thus, the spectrum of a metal porphyrin usually shows two bands in the visible region. In free-base porphyrins, two protons are linked to two opposite inner nitrogens (see Figure 1). In this case, the porphyrin plane no longer possess the 4-fold symmetry and β and α bands splits. In fact, the degenerate Q_o transition is replaced by transitions polarized along each of the nonequivalent *x* and *y* axes, Q_o^x and Q_o^y. Each transition has its vibronic envelope (Q_v^x and Q_v^y), and, as a consequence, four distinct bands characterize the spectrum of free base porphyrins in the visible region.[60−63]

The positions of the Soret, β, and α bands depend on the metal electron configuration, and the energy of the transitions varies as a consequence of the coupling between the metal and the porphyrin orbitals. The absorption spectra of metalloporphyrins are thus classified into three types, *normal*, *hypso*, and *hyper*.[63] *Normal*-type spectra are observed for a majority of metalloporphyrins with closed-shell metal ions, where the relevant porphyrin π orbitals do not significantly interact with the metal orbitals. The Soret, α, and β bands are often found around 400, 570, and 530 nm, respectively. *Hypso*-type spectra follow the *normal* absorption pattern, but all bands are blue-shifted, due to filled metal d orbitals to porphyrin π^* back-donation. Metal ions that cause *hypso*-type spectra are limited to those of d^6-d^9 electron configurations. Finally, *hyper*-type spectra show charge-transfer bands in addition to a significant red-shift of the porphyrin $\pi-\pi^*$ bands. They are difficult to analyze because the number of extra bands varies from one metal ion to another and the positions of all bands are far more dependent on the axial ligands than in the other types.[63]

Metal ions with d^1-d^5 electron configurations show these *hyper*-type spectra. Most of them can be easily found in lower oxidation states within the porphyrin, causing *normal*- or *hypso*-type spectra. Mn(III)− and Fe(III)−porphyrins are the best known examples in this respect.

The UV−vis spectra of heme−proteins show absorption patterns quite similar to those observed in simple metalloporphyrins. They are very sensitive to the oxidation and spin state of the iron, which are modulated by the protein environment. In addition to the Soret, β, and α bands, four extra bands are found in the lower energy of the visible region, and they are usually referred to as IV, III, II, and I. The typical UV−vis absorption data for several hemoproteins are reported in Table 1.[61,64−67]

II. Covalent Peptide−Porphyrin Systems

Several laboratories are presently investigating peptide-based heme−protein models in which the heme cofactor is covalently linked to one or two peptide chains.

The covalent attachment of ligands to the porphyrins is often desirable as it reduces axial ligand dissociation and scrambling, in those cases involving mixed axial ligation.

The pioneering works of Traylor and co-workers have contributed valuable information about the factors that allow the reversible dioxygen binding in hemoglobin and myoglobin.[33,34]

In 1962 Wang reported that simple porphyrin−imidazole mixtures could reversibly be oxygenated when immobilized in a polymer matrix.[68] Following this discovery, Traylor originated the idea that models of oxygen carriers should have one side protected with a hydrophobic structure (the *protected heme* approach) and/or a covalently attached proximal base on the opposite side (the *chelated heme* approach). These two features could ensure stabiliza-

Table 1. Typical UV–vis Absorption Data for Several Hemoproteins

			Soret		β		α	
protein	axial ligands	spin state	λ_{max} (nm)	$\epsilon \times 10^{-3}$ (M^{-1} cm^{-1})	λ_{max} (nm)	$\epsilon \times 10^{-3}$ (M^{-1} cm^{-1})	λ_{max} (nm)	$\epsilon \times 10^{-3}$ (M^{-1} cm^{-1})
			sperm whale Mb[a]					
MbO_2	His/O_2	LS	418	128	543	14.6	581	13.6
MbCO	His/CO	LS	423	187	542	14.0	579	12.2
Mb	His/H_2O	HS	434	115	556	11.8	588	s[g]
			horse Hb[b]					
HbO_2	His/O_2	LS	415	129	540	14.1	576	14.9
HbCO	His/CO	LS	419	192	539	13.9	569	13.9
Hb[h]	His/H_2O	HS	430	130	555	12.9	590	s[g]
cyanomet-Hb	His/CN	LS	422	114	542	10.9	575	s[g]
aquomet-Hb[i]	His/H_2O	HS	405	169	500	9.0	540	s[g]
			cytochromes					
E. coli b_{562} red[c]	His/Met	LS	427	180	531	17.6	562	32.1
E. coli b_{562} ox[c]	His/Met	LS	419	117	531	11.3	564	9.30
chloroplast b_{559} red[d]	His/His	LS	427		530		559	
chloroplast b_{559} ox[d]	His/His	LS	413		534		562	
michrosomes b_5 red[a]	His/His	LS	423		527		555	
michrosomes b_5 ox[e]	His/His	LS	413	117	530	11.0	560	9.16
P450–CAM[f]	Cys/H_2O	LS	417	115	536	10.6	569	11.1

[a] Data from ref 61. [b] Data from ref 62. [c] Data from ref 64. [d] Data from ref 65. [e] Data from ref 66. [f] Data from ref 67. [g] s indicates that the band produces a shoulder. [h] The III and I bands are detected at 758 nm (ϵ = 375 M^{-1} cm^{-1}) and 910 nm (ϵ = 195 M^{-1} cm^{-1}), respectively, and are diagnostic for the HS state. [i] The IV and III bands are detected at 580 nm (ϵ = 3400 M^{-1} cm^{-1}) and 633 nm (ϵ = 3900 M^{-1} cm^{-1}), respectively, and are diagnostic for the HS state.

tion of a five-coordinate heme complex and reversible oxygenation without competing oxidation.[33,34] Traylor and co-workers, followed by Collman, Momenteau, and Reed, reported on the use of the above-mentioned approaches for the development of dioxygen-binding molecules.[35,36] These molecules are essentially made up of a proximal base (pyridine, imidazole) covalently bound to the propionic group of pyrro-, proto-, meso-, or deuteroheme (see Figure 1) through an aliphatic linker of different length, suitable for positioning the axial ligand in the correct position for coordination. More efficient systems also contain a bulky moiety covering the opposite face of the heme. The bulky moiety prevents the formation of *hexa*-coordinated species and inhibits bimolecular reactions; further, it could represent a cavity to accommodate dioxygen. Some of these molecules were actually found to reversibly bind dioxygen, and it was possible to isolate and structurally characterize some stable dioxygen complexes at low temperature. Chelated and capped heme-based models did not find a widespread application, mainly due to their low stability at room temperature. However, they had an enormous impact on understanding the structure–activity relationships in the ligation of heme with dioxygen and carbon monoxide. They are milestones to demonstrate the importance of covalently derivatized porphyrin rings and to set the stage for the development of more sophisticated models that will be discussed in this section.

Quite different strategies were used for developing covalent peptide–porphyrin systems.

Microperoxidases are obtained by proteolytic digestion of cytochromes *c*.[69–75] Even though their molecular architecture was not derived by design approach, microperoxidases are important examples of structurally and functionally defined covalent peptide–porphyrin systems. They are often used for comparative analysis with newly developed designed heme–protein models, and therefore, their main properties will be reviewed in this paper.

In the first synthetic peptide–porphyrin conjugates, the porphyrin ring was covalently incorporated into peptide sequences in an effort to induce α-helical folding.[76,77] The helichrome developed by Sasaki and Kaiser[76,77] and the tetraphilins developed by DeGrado and co-workers[78] are successful models in which the porphyrin ring is able to direct the peptide folding into four-helix bundles. The important class of peptide-sandwiched mesohemes, developed by Benson and co-workers, also used a porphyrin template for inducing helical conformations.[79] A quite different approach was used in the design of mimochromes.[32] A miniaturization process was applied to natural heme–proteins in an attempt to find the shortest peptide sequences, which could serve partly the same functions of the protein chain in the natural counterparts.

Finally, it is important to point out that the preparation of covalent peptide–porphyrin systems often involves complex multistep synthesis, which employs methodologies of solution- and solid-phase peptide synthesis, reverse proteolysis, gene expression, and organic synthesis. The synthetic procedures adopted and the improvements applied for obtaining tailor-made molecules with high efficiency will be also briefly examined in the following paragraphs.

A. Microperoxidases

The term microperoxidases is used to define the range of heme–peptide fragments that can be obtained by the proteolytic digestion of cytochromes *c*. The microperoxidases framework consists of a small peptide fragment, containing the Cys-$(Xaa)_2$-Cys motif, covalently linked to the heme *c* through thioether linkages with the two Cys residues. The amino acid sequence of the polypeptide chain in

A

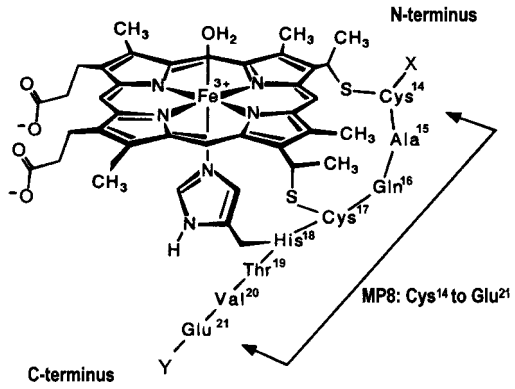

B

Derivative	X	Y
MP9	H	Lys
MP11	H-Val-Gln-Lys	OH
Fmoc-Pro-MP8	Fmoc-Pro	OH
Pro-MP8	H-Pro	OH
Pro_2-MP8	H-Pro-Pro	OH
MP9-22ε-(FmocAlaPro)	H	Lys(Fmoc-Ala-Pro)OH

Figure 2. (A) Schematic representation of the microperoxidase framework, depicted as six-coordinated aqua complex; the sequence of MP8 is indicated. (Reprinted with permission from ref 84. Copyright 1996 American Chemical Society.) (B) Some of the various microperoxidase fragments that can be obtained by selective proteolysis of cytochrome *c*, together with covalently modified derivatives.

microperoxidases is numbered according to that of the parent cyrochrome *c*; thus, the two Cys residues occupy positions 14 and 17 of the peptide chain. Selective proteolysis of cytochrome *c* affords various microperoxidases, differing in the peptide chain length.[69,70] The nomenclature used to describe microperoxidases is shown in Figure 2.

Several methods were reported for the preparation of microperoxidases starting from cytochrome *c*. Generally, the trypsin digestion of cytochrome *c* leads to MP8 while pepsin degradation gives MP11.[71] Recently the preparation of mutant microperoxidase decapeptides (MP10s) was achieved by reverse proteolysis reactions.[72] It was reported that trypsin is effective in catalyzing peptide bond formation when MP9 acts as substrate in 50% aqueous dimethylformamide solution with an excess of an amino acid, as incoming nucleophile. Using this procedure microperoxidase decapeptides with C-terminal His, Tyr, and Met were obtained in reasonable yields.[72]

The structure of microperoxidases is very appealing, since these small molecules contain the minimal requirements for an heme−protein mimetic. They bear a His residue at position 18, which coordinates the iron and acts as proximal ligand. In addition, the sixth coordination site is open, thus allowing the accommodation of exogenous ligands or substrates. Owing to these properties, microperoxidases are very useful models for the analysis of the spectral, magnetic, ligand-exchange, and catalytic properties of heme−proteins. The most thoroughly studied among the microperoxidase family is MP8. Its spectroscopic properties were widely investigated by means of several techniques, and electronic, CD, NMR, and EPR data are available for this molecule. One of the major drawbacks in the use of microperoxidases is that they show a tendency to aggregate in aqueous solution.[71] This phenomenon limits the practical applications of these heme−peptide fragments, since they can exist in solution as a mixture of multiple species. The origin of this process was deeply investigated on MP8, and two main factors are responsible for the aggregation: (1) intermolecular coordination via the free N-terminal group of one heme−peptide chain, which occupies the sixth axial position of another heme−peptide,[70,73] and (2) noncovalent $\pi-\pi$ interaction between two exposed heme groups.[74,75]

The absorption features of ferric and ferrous MP8, in both the aggregated and monomeric forms, were determined as a function of pH, solvents, and exogenous ligands.[71,80,81]

Monomeric solutions of MP8 in aqueous buffer can be obtained at very high dilution ($<10^{-6}$ M);[71] at this concentration, in the pH range 7.5−13, the absorption spectrum of MP8 is consistent with the presence of a high-spin species (see Table 2).[80] At 10^{-5} M it becomes dimeric, retaining a high-spin state, while further aggregates with a low-spin state are detected at MP8 concentrations higher than 10^{-4} M.[71,75] The use of solvent mixtures and the addition of ligands or detergents, which disperse these aggregates, strongly reduce intermolecular interactions. UV−vis, NMR, and resonance Raman studies of both ferric and ferrous MP8 and MP11, in micelle solutions, were reported.[80−82] In these solutions the heme−peptide systems appear to be monomeric; thus, their coordination properties as a function of pH can be determined. At very low pH the heme−peptides show a high-spin *bis*-aquo coordination; as the pH is increased (≈6), the complexes exist as a high-spin *mono*-histidine *mono*-aquo species. Finally, at extremely high pH, the low-spin histidine−hydroxo complexes are observed. Spectrophotometric tritations showed that MP8 and MP11 can bind one or two molecules of exogenous ligands, forming *mono*- and *bis*-ligated complexes.[80−82] Thus, they represent good model systems for the analysis of the spectral and magnetic properties of the various mixed-ligand states that can be found in natural heme−proteins (compare Tables 1 and 2).

More recently, the preparation of chemically modified microperoxidases emerged as an alternative strategy to overcome the problem of their aggregation in aqueous solution.[83−86] Munro and Marques reported a detailed analysis of the solution chemistry of *N*-acetyl-MP8 and demonstrated that MP8 can be successfully acetylated.[84,86] In fact, treatment of MP8 with 500 molar excess of acetic anhydride, in aqueous buffer at pH 9.3, resulted in a nearly 100% conversion of MP8 into AcMP8. The presence of the *N*-acetyl group in MP8 strongly reduces its aggregation behavior, since AcMP8 exists as monomeric species in aqueous solution up to 3×10^{-5} M concentration.[83−85] All the data clearly indicate that protection of the

Table 2. Absorption Maxima of Several Microperoxidase Derivatives

species	axial ligand	spin state	Soret (nm)	solvent
MP8[a]	His/H_2O	HS	399	CTAB, pH= 7.5
MP8[a]	His/H_2O and His/OH^-	IS[f]	403	CTAB, pH= 13
MP8[a]	His/Im	LS	407	CTAB, pH= 7.5
MP8[b]	His/CN	LS	410	methanol
MP8(II)[a,g]	His/H_2O	HS	428	CTAB, pH = 7.5
Ac-MP8[c]	His/H_2O	HS	396	aqueous buffer, pH = 7.0
Ac-MP8[c]	His/OH^-	LS	405	aqueous buffer, pH = 12.8
MP11[d]	His/H_2O	HS	395	SDS, pH=6.5
MP11[d]	His/ OH^-	LS	408	SDS, pH ≥ 10
MP11(II)[d,g]	His/H_2O	HS	430	SDS, pH = 9.8
Ac-MP11[e]	His/H_2O	HS	397	aqueous buffer, pH = 7.5
Ac-MP11[e]	His/Im	LS	406	aqueous buffer, pH = 7.0
Ac-MP11[e]	His/CN	LS	412	aqueous buffer, pH = 7.0

[a] Data from ref 80. [b] Data from ref 97. [c] Data from ref 84. [d] Data from ref 82. [e] Data from ref 86. [f] IS indicates intermediate spin state. [g] (II) refers to the ferrous state.

Cys[14] α-amino group on MP8 excludes intermolecular coordination between two heme−peptide fragments. Thus, aggregation phenomena that are observed at higher heme−peptide concentrations can be attributed to $\pi-\pi$ interactions between heme groups.[85] In addition, the coordination properties of Ac-MP8, as a function of the pH, revealed that this system remains six-coordinated in solution and the axial ligand combination is critically dependent on pH, as reported in Table 2.[83,84] Treatment with acetic anhydride converts MP11 into the *bis*-*N*-acetyl derivative, which exhibits a much lower tendency to aggregate in aqueous solution than its precursor.[86] This molecule is in fact very soluble in aqueous media, existing as a monodispersed system at concentrations of at least 6×10^{-4} M. In addition, it shows a good affinity toward exogenous ligands, and mixed-ligand species can be easily prepared.

MP8 and MP11, along with their derivatives, were shown to be effective catalysts in oxidation and oxygenation reactions. Adams and Goold reported kinetic investigations on the peroxidase activity of MP8 by using ABTS as reducing substrate.[87,88] These results confirmed previously reported studies and indicated that the activation of hydrogen peroxide by MP8 proceeds via the formation of a high-valent iron−oxo intermediate analogous to peroxidase compound I.[3] This active heme intermediate can react with the substrate to yield the product, but it can also be deactivated with resulting bleaching of the catalyst.

Cunningham and co-workers analyzed the kinetics of the peroxidase activity of MP8 by using a range of organic substrates, such as aniline, naphthols, and phenols.[89−91] Their results confirmed that MP8 is able to catalyze the oxidation of a wide number of organic substrates in a peroxidase-like reaction, although the nature of the oxidized intermediate formed in the reaction can be different from that produced by the natural proteins.

Recent work demonstrated that MP8 could mediate cytochrome P450-like oxygen-transfer reactions.[92−95] Rietjens and co-workers analyzed the mechanism of aromatic hydroxylation of aniline by the MP8/H_2O_2 system.[92] Analysis of the monoxygenation reaction of aniline, by using ^{18}O-labeled hydrogen peroxide, strongly supports the aromatic hydroxylation catalyzed by MP8 proceeding through a mechanism that resembles the peroxide shunt pathway of cytochrome P450.[3,37]

Despite the wide variety of reactions they catalyze, the applications of microperoxidases as minicatalysts are limited by their low stability under catalytic conditions. Accessibility of the distal side causes degradation of the porphyrin ring during catalysis, either by the direct action of H_2O_2 or by intermolecular reactions with another active iron−oxo species. However, their stability is higher than simple protoporphyrin systems, thus indicating that the presence of the small peptide chain can play an important protective role toward the bleaching of the catalyst. This finding was proven by the analysis of the kinetics of aniline hydroxylation, catalyzed by microperoxidases that bear peptide chains of different length.[96] An increase in the size of the attached peptides results in an increase of catalyst stability. Several mechanisms may account for the protective role of the peptide chain since it could either (i) function as a scavenger for hydroxyl or superoxide radicals, (ii) make a barrier for the formation of the inactive μ-oxo diiron dimer, or (iii) act as an alternative source of H atoms, thus reducing the inactivation of the microperoxidases by H-atom abstraction from the *meso* position of the porphyrin ring. A definitive answer for this will come when detailed structural information about the interaction between the peptide and the heme group will be available. The tendency of microperoxidases to aggregate strongly limited their structural characterization by NMR. Poor resolution spectra were obtained with MP8, both for the aggregation phenomenon and for the presence of the high-spin iron center. This problem was recently solved by Gray, Duus, and co-workers, who reported the paramagnetic NMR characterization of the low-spin ferric−cyanide MP8 derivative in methanol solution.[97] One of the most striking pieces of evidence that the heme−peptide fragment retains some of the structural features of the parent heme−protein is that the pattern of the heme methyl resonances resembles that found in the cyanoferric heme *c* proteins. Further, the imidazole side chain of His[18] is coordinated to the iron center with a fixed orientation. All the data indicate that while the C-terminal tail is very flexible, residues 14−18 form

a rigid loop which resembles the one, highly conserved, found in the native *c* cytochromes. The finding that in MP8−CN the position of the imidazole ring, relative to the heme, is preserved even in the absence of the entire protein suggests that the 14−18 loop dictates the axial ligand orientation. Thus, this small peptide fragment can play an important role in modulating the reactivity of the heme.

The effect of the peptide chain in modulating the properties of the heme group was also investigated by preparing covalently modified microperoxidases. Casella and co-workers reported the aggregation behavior and catalytic activity of MP8 and MP9 covalently modified by the attachment of one or more amino acids to the amino-terminal position of the peptide chain.[98] In particular, Fmoc-Pro-MP8, Pro-MP8, Pro_2-MP8, and a variant of MP9, in which the Fmoc-Ala-Pro peptide has been linked to the ϵ-amino group of Lys22, were studied in the catalysis of *p*-cresol oxidation by hydrogen peroxide. Under the experimental conditions employed, the reaction rates were found to be independent of substrate concentration and linearly dependent on both H_2O_2 and catalyst concentrations. Thus, the rate-determining step of the reaction is the formation of the high-valent state of the catalyst. Two main factors are important in controlling this step: the steric hindrance at the distal side and the need of acid−base catalysis in the heterolytic cleavage of the peroxide. Among the systems investigated, Pro_2-MP8 showed the best catalytic performance. In fact, the presence of a single Pro residue causes Pro-MP8 to be 2-fold more active than MP8; the addition of a second Pro residue, in Pro_2-MP8 derivative, further increases the catalytic efficiency. This finding could be explained by considering that the proline amino group could come in close contact with the iron-bound peroxide, thus promoting its cleavage.

MP8 is able to catalyze other cytochrome P450-like common reactions, such as sulfide oxidation and O- and N-dealkylation.[99,100] More interestingly, new activities were very recently reported for this molecule, such as the formation of Fe(II)−nitrosoalkane complexes.[101]

All these findings support the use of MP8 and the other microperoxidase derivatives as real model systems for their natural counterparts, i.e. peroxidases and cytochrome P450s. It is clear, by the large amount of data reported in the literature, that these systems could be used as mini-enzymes for several applications. New applications were recently envisaged, such as their use in the construction of hydrogen peroxide biosensors.[102] Moreover, microperoxidase features have strongly highlighted the role of the peptide chains in modulating the reactivity of the heme ring,and have stimulated the design toward minicatalysts based on covalent peptide−porphyrin systems.

B. Chelated Deuteroheme Complexes

Casella and co-workers first reported synthetic deuteroheme−peptide conjugates in an attempt to study how peptide sequences influence the heme reactivity.[103−108] The molecular models of these deuteroheme complexes, developed as both *mono*-peptide and bispeptide adducts, are shown in Figure 3.

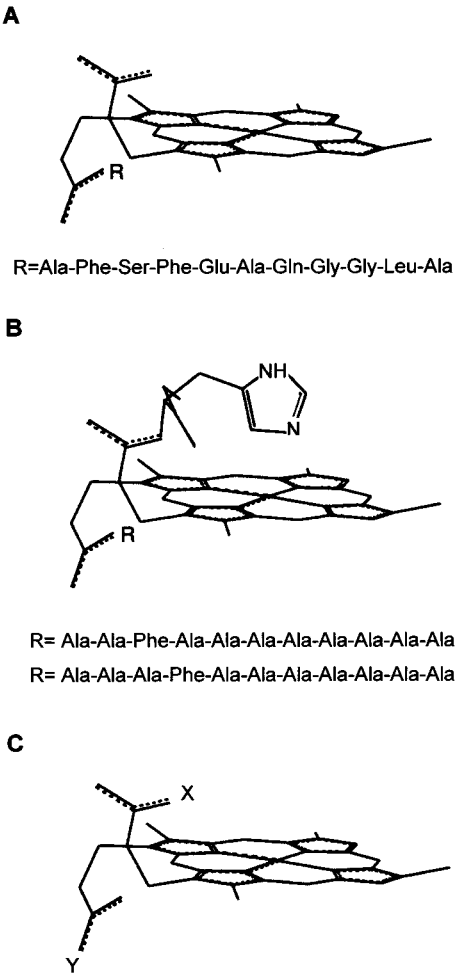

Derivative	X	Y
DH-H	HisOMe	OH
DH-AH	AlaHisOMe	OH
DH-GH	Gly-HisOMe	OH
DH-bisGH	Gly-HisOMe	Gly-HisOMe

Figure 3. Molecular structures of chelated deuteroheme complexes: (A) deuteroheme undecapeptide; (B) chelated deuteroheme undecapeptide; (C) chelated deuteroheme.

The covalent modification of deuteroheme with different peptides was simply achieved by employing the solution methods of peptide synthesis.[103,104] The synthesis of the chelated deuteroheme *mono*-peptide complexes usually afforded a mixture of two products containing the peptide linked at either position 2 or 18 of deuteroheme. Only in a few cases were these structural isomers separated; otherwise the isomer mixture was studied.

In the first molecule developed, an undecapeptide was covalently N-terminally linked to the propionic group of deuteroheme (Figure 3A).[103] This medium-sized peptide contains polar and acidic residues, which should confer solubility to deuteroheme in a protic medium. The presence of the peptide chain strongly influences the binding and catalytic properties of deuteroheme. First, titration of deuteroheme−undecapeptide with imidazole, followed by visible

spectroscopy, showed that the complex binds up to two imidazoles. The binding equilibrium occurred in two steps: the first imidazole binds with high affinity, while the affinity for the second imidazole is markedly lower. The authors hypothesized that the folding of the peptide chain in the *mono*-imidazole adduct greatly limits the accessibility to the sixth iron coordination position. The catalytic properties of the deuteroheme−undecapeptide complex in peroxidase- and catalase-like reactions were investigated by using thioanisole or tyrosine as substrates and hydrogen peroxide as oxidant. In the catalytic oxidation of D- and L-tyrosine, the complex exhibited some stereoselectivity ascribed to specific interactions between the substrate and the peptide chain.

In subsequent works, the same investigators developed chelated deuteroheme complexes in an effort to study the effects of the axial ligand on the catalytic properties of deuteroheme.[104] In these new systems, a histidine methylester or a histidine containing dipeptide, covalently linked to one of the two propionic groups, constituted the chelating arm (Figure 3B). A different peptide chain was linked to the second propionic group; the peptide sequence was rationally chosen with the aim of evaluating the effect of specific amino acids in inducing stereoselective oxidation.

Two complexes, each containing a different phenylalanyl−polyalanine sequence, were studied (Figure 3B).[104] The kinetic parameters for the catalytic oxidation of D- and L-tyrosine, using *tert*-butyl hydroperoxide, revealed a marked difference in the chiral discrimination ability of the two complexes. A moderate chiral discrimation was observed only when the Phe residue is placed at position 4 of the peptide sequence (Figure 3B). Therefore, the Phe position seemed to be important for chiral discrimination.

The analysis of the axial-ligand distortion effects on the catalytic and binding properties of deuteroheme was investigated by examining the behavior of complexes bearing short chelating arms: DH−His, DH−Ala-His, and DH-Gly-His (Figure 3C).[105,106] Molecular mechanics calculation revealed the length of the chelating arm critically affects the coordination. The presence of two amino acid residues in the chelating arm causes less strain in the axial coordinative bond with respect to the DH−His complex. The strain energy influences the catalytic and binding properties of the metal center, as a consequence of an altered electron distribution in the strained complex.

Chelated deuteroheme complexes were also used in the construction of cytochrome *c* oxidase models.[107,108] These systems are based on DH−His or DH-Gly-His, which have been covalently modified by coupling a chelating ligand for copper to the second free porphyrin propionic group (Figure 4). A *bis*-benzimidazole arm constitutes the copper binding site. The resulting heterodinuclear complexes, named DH−HBB/Cu and DH-GHBB/Cu, were studied as mimetics of the dioxygen reduction center found in the cytochrome *c* oxidase.[109]

Both complexes bind Cu^{2+}, and interestingly their EPR spectra, recorded in frozen DMSO solutions at 123 K, are different. In particular, the spectrum of DH−HBB/Cu is characteristic of Cu(II) in tetragonal

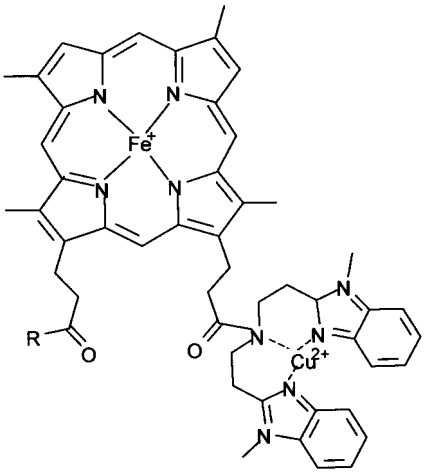

Derivative	R
DH-BB/Cu	OH
DH-HBB/Cu	HisOMe
DH-GHBB/Cu	GlyHisOMe

Figure 4. Chemical structures of cytochrome *c* oxidase models. (Adapted from ref 108.)

symmetry while that of DH-GHBB/Cu appears to be rhombic. These differences can be ascribed to the presence of intramolecular Fe−Cu interactions in the latter complex, which are mediated by bridging solvent molecules. The redox behavior of the dinuclear complex is quite remarkable. Addition of ascorbate causes the selective reduction of Cu(II) to Cu(I). This finding may demonstrate that the redox potential of the copper center is higher than that of the iron center, as found in cytochrome *c* oxidase. Treatment of the complexes with excess dithionite gave the fully reduced Fe(II)/Cu(I) complex, which is able to react with dioxygen, giving the fully oxidized Fe(III)/Cu(II) species. However, the most promising complex is DH-GHBB/Cu since only with this complex does the oxidative reaction proceed at room temperature without any oxidative decomposition of the porphyrin.

C. Peptide-Sandwiched Deuteroheme: Mimochromes

Our laboratory has approached the challenge of constructing heme−protein models using a miniaturization process.[32] A miniaturized heme−protein is a peptide-based model which contains a minimum set of constituents necessary for (i) an accurate reconstruction of a well-defined structure and (ii) a fine-tuned reproduction of a defined function. This strategy leads to the development of a class of miniaturized heme−proteins, named mimochromes.[110−114]

The main features of mimochromes are the covalent structure and a well-defined helical conformation of the peptide chains linked to the deuteroporphyrin ring, even in the absence of metal ion coordination. The schematic structures of mimochromes are reported in Figure 5.

A minimalist approach was used to design short peptide sequences which could serve partly the same

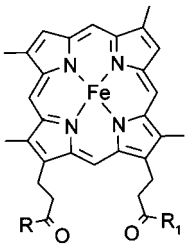

Mimochrome		R, R1
I	R=R1	Ac-L-A-Q-L-**H**-A-N-*K*-L-NH2
II	R=R1	Ac-D-L-S-D-L-**H**-S-K-*K*-L-K-I-T-L-NH2
IV	R=R1	Ac-E-S-Q-L-**H**-S-N-*K*-R-NH2
III, V, VI	R≠R1	R= Ac-D-E-H-K-L-**X**-S-K-*K*-R-K-I-T-L-NH2
		R1= Ac-D-E-H-K-L-**Y**-S-K-*K*-R-K-I-T-L-NH2

X= H, or α-amino-δ–mercapto-pentanoic acid
Y= G, A or S

Figure 5. Schematic representation of the chemical structures of mimochromes. The covalent linked K residue is indicated in italic, and the axial ligand is indicated in bold.

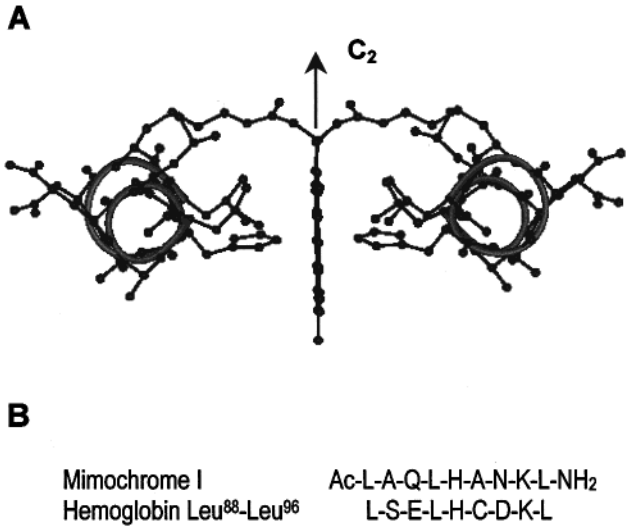

Figure 6. (A) Molecular model of mimochrome I, showing the C_2 symmetry axis. (B) Comparison of the amino acid sequences of mimochrome I and of the Leu[88]-Leu[96] hemoglobin fragment.

functions of the protein chain in the natural heme–proteins.[110,112] A detailed analysis of heme–protein structures showed that the prosthetic group in natural heme–proteins is strongly kept inside the protein structure by a large number of interactions. These interactions were replaced in mimochromes by a few strong local constraints. The prototype molecule, mimochrome I, was patterned on the F helix of hemoglobin β-chain.[115] The smallest sequence, required for a complete coating of one face of the heme, was identified in a nine-residue peptide, which contains a central His residue to ligate the heme iron. Leu residues were placed at positions i−4 and i+4 relative to the His to hydrophobically interact with the heme macrocycle. Two copies of the peptide were covalently linked to the porphyrin propionic groups through the ϵ-amino function of Lys,[8] obtaining a *pseudo*-C_2-symmetric dimer (Figure 6).[110]

The spectroscopic and structural characterization of mimochrome I indicated that it binds cobalt and iron in a low-spin *bis*-His-ligated state, as envisioned in the design. Interestingly, the insertion of metal ion into the porphyrin ring gave two diastereomeric forms, differing for the configuration around the metal ion; the two exchange-inert Co(III) complexes were separated by RP-HPLC and separately analyzed. The UV–vis pH titration showed that the iron *bis*-His coordination is strong enough to bring the His p*K* value around 2.5. The *bis*-His coordination is even stronger in Co(III) complex, and it occurs at a pH ≥ 1.8.[111] This unexpected low His p*K* value confirms that in the designed molecule the peptide chains determine a highly hydrophobic local environment around the heme, which increases the coordination strength of the axial ligands. CD spectra in the far UV region confirmed the peptide chain to be predominantly in an α-helical conformation in both the *apo* and metalated species, even at low TFE concentration (10%). The induced Cotton effects observed in the Soret region for the iron and cobalt derivatives showed different shapes.[110,111] In particular, a double inflected spectrum was observed for the iron derivative and a negative or positive band characterized each of the two stable Co(III) forms (see Table 3). These remarkable differences are the first experimental evidence of the existence of two diastereomeric forms. The flexibility of the linker between the peptide and the deuteroporphyrin ring allows each peptide chain to be positioned either above or below the porphyrin plane (Figure 7). These arrangements produce enantiomeric configurations around the metal center. Because of the substituents on the porphyrin ring and the chirality of the peptide chain, the Δ and

Table 3. CD Parameters for Mimochrome Derivatives[a]

	UV region	Soret region	
	$[\theta]_{222}$	$[\theta]$	sign
mimochrome I	••	not detected	
Fe(III)–mimochrome I	••	(−) •••; (+) •	S-shaped
Co(III)–mimochrome IΔ	••	•••••	negative
Co(III)–mimochrome IΛ	••	•••	positive
mimochrome II	•••	not detected	
Co(III)–mimochrome II	•••	••	negative
mimochrome III	•••	•	negative
Fe(III)–mimochrome III	•••	••	positive
mimochrome IV	•	not detected	
Fe(III)–mimochrome IV	••	••••	positive
Co(III)–mimochrome IV	••	•••	positive

[a] The intensities of the cotton effect are proportional to the number of •.

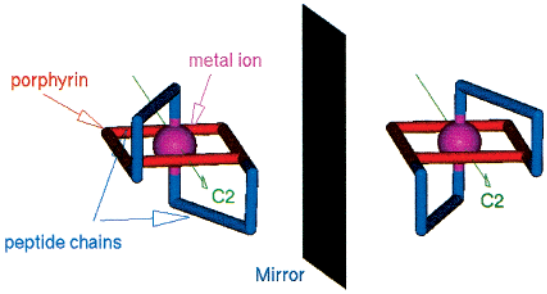

Figure 7. Schematic representation of the two possible orientations of the peptide chains around the metal center, which give rise to the two Δ and Λ diastereomers.

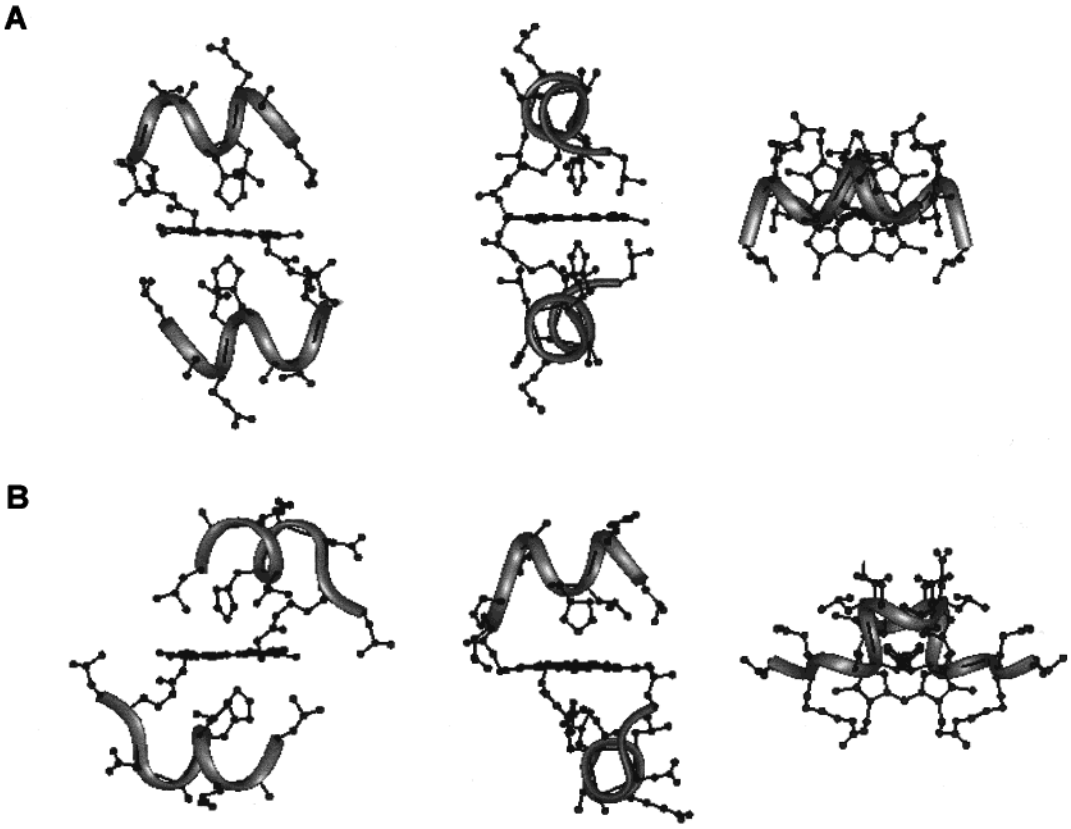

Figure 8. Front, side, and top views of the average molecular structures obtained from NMR experimental data and RMD calculations for (A) Co(III)−mimochrome I Δ isomer and (B) Co(III)−mimochrome I Λ isomer.

Λ isomers of Co(III) mimochrome I are indeed diastereomers.

This finding was confirmed by the solution structural characterization.[111] In fact, the NMR structures of the two diamagnetic Co(III) isomers (Figure 8), which represent the first example of structure determination of a designed heme−protein models, allowed a definitive identification of the two isomers as the Δ and Λ diastereomers and a straightforward correlation between their structure and spectral properties. As expected, the peptide chains adopt an almost regular α-helical conformation; the helices lie parallel to the porphyrin plane, and they are antiparallel to each other in the Δ isomer and about orthogonal in the Λ isomer (see Figure 8).

The analysis of the three-dimensional structure of the two cobalt isomers was important in understanding the properties of the Fe(II) and Fe(III) complexes, which could not be studied by NMR spectroscopy because of their poor solubility. The remarkably different solubility between the iron and cobalt complexes was tentatively attributed to the simultaneous presence of the two diastereomers, for the iron complex, in fast interconverting equilibrium. During this process both peptide chains might be displaced from the porphyrin plane. The porphyrin ring is thus exposed to the solvent, and aggregation by stacking of the porphyrin ring may occur. Confirmation for this hypothesis came from the CD spectral properties in the Soret region, which are an average of those corresponding to the two separate diastereomers (see Table 3).

The unpredicted but experimentally observed Λ and Δ isomers of Co(III)−mimochrome I clarify the concept of diastereomerism that may occur when polypeptides coordinate to metal ions. The use of local *pseudo*-C_2 symmetry is particularly advantageous to construct symmetric molecules with minimized size, because it simplifies the design, reduces the size of the molecules to be synthesized, and may simplify their structural characterization.[116,117] However, great attention should be paid in the design to overcome the problem of diastereomer formation.

The information derived from mimochrome I was fruitfully applied for improving the design, which focused on molecules with longer (14 residue) sequences, modeled in both α-helical (residues 1−10) and extended (C-terminal part) conformations.[112] Interestingly, a unique diastereomer was stabilized in both iron and cobalt derivatives. Further, the newly developed molecules show a higher helix content with respect to mimochrome I, even in water. These findings confirm the correctness of the design and show that all the changes made in the sequence not only stabilize a single topology of the peptide chains around the porphyrin but also favor helix formation with respect to mimochrome I.

The last achievement was the design of molecules capable of stabilizing a five-coordinate iron(II) complex, providing an empty site available for catalyzing oxidation reactions.[114] The axial-coordinating His, in one chain, was replaced with a smaller residue (see Figure 5) unable to coordinate the metal, thus creating a cavity near the metal center. The local environment around the metal center is mainly hydrophobic, and to stabilize the reduced state for the iron ion, several positively charged residues were inserted in the solvent-exposed positions. Moreover, interchain

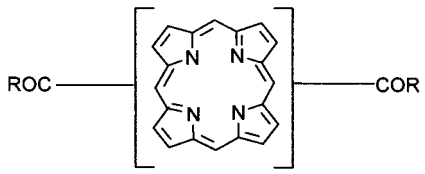

PSM derivative	Porphyrin	R
1	Mesoporphyrin IX	Ac-A*K*EAA**H**AEAAEAACONH$_2$
2	Mesoporphyrin IX	Ac-AAEAAEA**H**AAE*K*ACONH$_2$
3	Mesoporphyrin IX	Ac-A*K*EA**H**AAEAAEAACONH$_2$
4	Mesoporphyrin IX	Ac-AAEAAEAA**H**AE*K*ACONH$_2$
5	Mesoporphyrin IX	Ac-AA**H**AEAAEA*K*EAACONH$_2$
6	Mesoporphyrin II	Ac-AAEAAEA**H**AAE*K*ACONH$_2$
7	Mesoporphyrin II	Ac-AAEFAEA**H**AAE*K*ACONH$_2$
8	Mesoporphyrin II	Ac-AAEWAEA**H**AAE*K*ACONH$_2$

Figure 9. Schematic representation of the chemical structures of peptide sandwiched mesoheme (PSMs). The covalent linked K residue is indicated in italic, and the H axial ligand is depicted in bold. *Mono*-peptide adducts, in which one R group is OH, were also prepared.

ion pairing residues were inserted into the sequence to further stabilize the sandwich structure.

The results obtained on this class of molecules indicate that simple, structurally defined systems provide a good opportunity for investigating how changes in the electrostatics, polarity, and solvent accessibility to the heme site affect the properties of the prosthetic group, such as the thermodynamics and rates of electronic transfer.

An important endeavor of this work was the development of a versatile strategy for the synthesis of covalent heme−peptide conjugates.[110,112] By using Fmoc solid-phase peptide synthesis, the porphyrin derivative was directly incorporated on the solid support. It is worth mentioning that the synthetic procedure allows a rapid preparation of a large variety of analogues, either with symmetric or unsymmetrical peptide chains. Thus, the effects of systematic variation in the peptide composition on the overall properties of the molecule could be rapidly investigated. Furthermore, the insertion of the metal in the final assembled peptide−porphyrin moiety allows analyzing a variety of metalloporphyrin complexes, without re-synthesizing the entire molecule.

D. Peptide-Sandwiched Mesoheme

In an independent series of contributions, Benson and co-workers also prepared a series of peptide-sandwiched mesoheme complexes, indicated as PSMs.[79,118−122] In PSMs the mesoheme II or IX is covalently linked to one or two peptide chains via an amide linkage between the propionate heme function and the N-ϵ nitrogen of lysine residues. A His residue in each peptide coordinates the heme iron, thus allowing the peptide chains to fold above and below the porphyrin ring, giving rise to a sandwich structure.[79] A schematic representation of the PSMs structures is reported in Figure 9.

One of the main features of PSM molecules is that a random coil−helix transition of the peptides occurs upon histidine to iron binding. The first derivatives of the PSMs series are characterized by the presence of a 13-residue peptide covalently linked to the mesoheme propionic groups (1 in Figure 9). The peptide was designed to have high helical propensity and to convey water solubility to the structure. A polyalanine sequence, containing Glu residues in the solvent-exposed position, was created. Lys and His were placed into the sequence to achieve the covalent linkage to the porphyrin and the iron coordination, respectively. They occupy positions i and i+4, respectively, with Lys close to the N-terminus.[79]

The synthesis of PSMs involves a minimun of steps. First, the peptides were synthesized by the standard solid-phase methods. The preparation of the bis-*p*-nitrophenyl ester of iron(III) mesoporphyrin IX allowed direct coupling of the unprotected peptides, through the Lys ϵ-amino function, to the porphyrin ring; changing the peptide equivalents relative to the porphyrin gave rise to the *mono*- or *bis*-adduct.

The folding behaviors of the free peptide and of the mesoheme derivatives 1 were deeply investigated by the use of CD spectroscopy. The free peptide showed a random coil conformation in water solution, whereas the *bis*-peptide mesoheme showed enhanced helicity relative to the free peptide. Increasing the amount of the α-helix-inducing solvent TFE enhanced the α-helical content for both the free peptide and the *bis*-peptide mesoheme complex. Acidification of the solution to pH 2 causes the peptide to assume a random coil conformation, due to the breaking of the iron−histidine axial bond.[79] This finding clearly demonstrated that the peptide helicity in this system results entirely from iron to histidine coordination. The covalent attachment of the peptides to the porphyrin is not sufficient to direct the α-helical folding; a coordinative bond is also required to position the peptide chains in close contact with the porphyrin and to favor the folding.

To rationalize the factors that impart stability to the PSMs molecules, new derivatives were developed.[118] By changing the Lys-His separation, the chelate effect and the resulting strain in the Fe−His axial bond were evaluated. In addition, in some derivatives, the position of Lys was changed from N- to C-terminus, i.e., reversed peptide sequences were synthesized. In particular, in the newly PSM derivatives, Lys and His were placed, respectively, at the following positions: i, i−4; i, i+3; i, i-3; i, i−7 (compound 2, 3, 4, and 5 in Figure 9, respectively).

The UV−vis, CD, and EPR analysis of both *mono*- and *bis*-peptide adducts revealed that stability of PSMs is controlled by several factors. In all derivatives His is able to coordinate the iron, giving rise to pentacoordinated high-spin species in the *mono*-adducts and low-spin hexacoordinated species in the *bis*-adducts. An important factor that modulates the stability of PSMs is the length of the chelating arm, i.e., the distance between Lys and His residues. The strongest coordination was found in compounds 1, 2, and 4, which showed quite reasonable helical contents even in the absence of organic cosolvents such as TFE and PrOH. On the other hand, derivatives 3 and 5 are less stable even when the cosolvents are used. All systems were studied in both the iron(II)

and iron(III) oxidation states. Interestingly, the Fe(II) complexes of 3 and 5 exist as a mixture of high-spin five-coordinate and low-spin six-coordinate species whereas 1, 2, and 4 remain six-coordinate in both Fe(II) and Fe(III) oxidation states.[118] This finding clearly demonstrated that different spacing between His and Lys causes a different stability of the overall structure.

In subsequent works, peptide−heme adducts based on the mesoporphyrin II were developed.[119−121] Even though they contain a C_{2h}-symmetric porphyrin, these new compounds still may present the problem of diastereomer formation, which arises from different arrangement of the peptide chains around the macrocycle. Introduction into the peptide sequence of aromatic residues, such as Trp and Phe, allowed evaluation of the aromatic interactions between porphyrin and peptides.[120,121] In particular, the sequence of PSM 2 was attached to mesoporphyrin II to give PSM 6. In addition, replacement of Ala^4 with Trp and Phe leads to PSM 7 and PSM 8, respectively (see Figure 9). Molecular modeling studies suggested that Trp residue could better stabilize the stacking interactions with the porphyrin ring with respect to Phe. A complete analysis by UV−vis and CD spectroscopies on both the iron and cobalt complexes was reported. All the Fe(III) complexes exist as low-spin hexacoordinate species. Lowering the pH causes the Fe−His axial bond to be broken. Thus, the analysis of the Soret band extinction coefficients as a function of pH allowed determining the relative stability toward acid for the three PSMs derivatives (6, 7, and 8). The pH tritation data showed an increased stability toward acid in the order 7 > 8 > 6. This indicated that the aromatic residues favor the *bis*-coordinated folded state and that this effect is more pronounced when the Trp residue is present in the sequence. Further, only the $Ala^4 \rightarrow Trp^4$ substitution caused an increase of the helical content.[121]

Structural information for these molecules was obtained from NMR characterization of the Co(III) diamagnetic complexes,[121] which have been already found to be amenable for NMR analysis.[111] One-dimensional ^1H NMR spectra, recorded in CD_3OD, showed that in PSM 7 and 8 the resonances of the Trp^4 and Phe^4 side chains are shifted upfield with respect to their normal positions, thus suggesting the presence of a strong interaction between these residues and the porphyrin ring. The upfield shift of these resonances is strongly enhanced by the addition of D_2O to the samples. This indicated that the increase in the polarity of the solvent causes the aromatic residues to interact more strongly with the porphyrin, thus suggesting that this interaction is mainly driven by hydrophobicity. The helices in PSM 7 are more highly organized that in PSM 6 and span the entire sequences. On the other hand, PSM 8 showed a helical arrangement only for the Phe^4-Ala^{13} segment.

The work on PSM molecules clearly confirms that in order to build a peptide-based heme−protein model with a well-defined three-dimensional structure, many factors should be taken into account. The covalent attachment of the peptide chains to the porphyrin ring may not result in the stabilization of the desired structure. The peptide sequences should be accurately designed in order to encompass all the essential elements for metal coordination and folding.

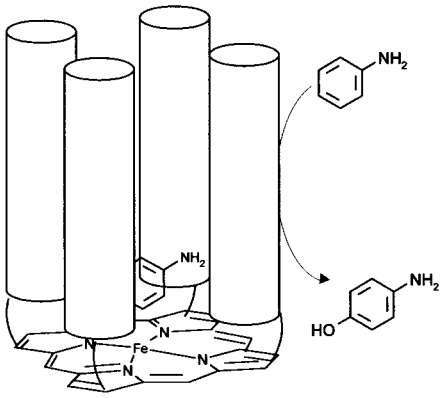

Figure 10. Schematic representation of the helichrome molecule.

A series of α-helical peptides covalently linked to heme were also studied by Mihara and co-workers.[123,124] In a recent paper they reported the development of two three-helix bundle proteins, 3α-H9 and 3α-H12, covalently bound to meso-heme IX as models of peroxidases.[124] The distal His ligand was placed in different positions within the two systems to regulate six- or five-coordination of the heme iron. The two molecules showed different activities toward the oxidation of *o*-methoxyphenol to *tetra*-guaiacol using hydrogen peroxide as oxidant. In particular, a good correlation was found between the coordination states of the heme and the catalytic efficiency of the systems, i.e., the molecule containing a higher content of five-coordination showed the best activity. However, the accessibility of hydrogen peroxide and its destructive effect toward the heme should be carefully balanced in order to enhance the activity.

E. Porphyrins as Templates for Inducing α-Helical Folding

The porphyrin ring has been successfully employed as a template for enhancing the α-helical content in peptides, helping to direct peptides to fold into four-helix bundles.[125,126]

The pioneering example of an artificial heme−protein, based on a peptide−porphyrin conjugate system, was developed by Sasaki and Kaiser in an effort of using a porphyrin ring as a template to direct helical folding into the attached peptides.[76,77] The resulting molecule, named "helichrome", is characterized by four identical 15-residue peptide chains N-terminally linked to the four propionic groups of coproporphyrin I, shown in Figure 1E. Helichrome was designed to mimic the hydroxylase activity of cytochrome P450, whose structure is characterized by the presence of several α-helices surrounding the heme group and forming a hydrophobic recognition site. Therefore, the peptide sequence in helichrome was chosen such that it could stabilize an amphiphilic helix and create, in the folded state, a substrate-binding hydrophobic pocket proximal to the porphyrin ring, as depicted in Figure 10.

Helichrome was synthesized employing the segment condensation approach, which was proven to be extremely useful for the assembly of the molecule. Using the oxime resin, it was possible to obtain the N- and C-terminus fragments (1−7 and 8−15) by the same synthetic intermediate upon treatment with 1-hydroxypiperidine and Leu amide, respectively. The resulting fully protected peptide, after removal of the N-terminus protecting group, was reacted with the activated porphyrin ester for 2 days at 50 °C. After side chain deprotection and purification, the desired peptide−porphyrin conjugate was obtained with a 37% yield. Iron was inserted into the porphyrin ring by the acetate methodology,[63] slightly modified, after the complete assembly of the molecule.

Structural and functional characterization showed that the metalloporphyrin moiety in helichrome serves both as a molecular constraint to prevent the complete collapse of the α-helical bundle and as a catalytic center. Helichrome shows quite remarkable features. First of all, it is water soluble above pH 3, as expected from its sequence, without concentration-dependent aggregation, observed for coproporphyrin. Further, the peptide chain exhibits a high α-helical content as assessed by CD measurements in phosphate buffer at pH 7.5. The four-helix bundle structure is induced and stabilized by the porphyrin template, since the isolated peptide segment adopts a random coil conformation, under identical experimental conditions. Further, in agreement with an intramolecularly folded state, gel filtration and analytical sedimentation equilibrium ultracentrifugation experiments revealed that helichrome is monomeric under the experimental conditions of the spectroscopic measurements. Finally, the guanidinium hydrocloride-induced unfolding was also monitored by CD spectroscopy to determine the stability of helichrome. The free energy of folding (−4.4 kcal mol^{-1}) was determined to be comparable to that of native globular proteins.[77] The aniline hydroxylase activity of the helichrome−iron(III) complex was also examined by monitoring the formation of *p*-aminophenol as a function of the aniline concentration.[76] Surprisingly, helichrome was found to have aniline hydroxilase activity, using O_2 as oxidant, in the presence of fixed 7-acetylflavin and NADPH concentrations at pH 7.0. The resulting k_{cat} and k_m values (0.02 min^{-1} and 5.0 mM, respectively) are similar to those of natural heme−proteins that possess this activity (k_{cat} and k_m ranging from 0.02 to 0.65 min^{-1} and from 3.7 to 5.4 mM, respectively).[76] Interestingly, the rigid hydrophobic pocket formed by the peptide chains plays a key role for helichrome activity because the iron(III) complex of the isolated coproporphyrin showed negligible catalytic activity under the same conditions.

A quite similar approach was followed by DeGrado and co-workers in the development of tetraphilins (see Figure 11).[78] These molecules were designed with the aim of mimicking the activity of ion-channel proteins. To provide assemblies of defined aggregation state and drive amphiphilic peptides into four-helix bundles, ion-channel-forming peptides were covalently attached to a tetraphenylporphyrin derivative (shown in Figure 1F). Tetraphenylporphyrin was preferred for its major rigidity and chemical stability when compared to the coproporphyrin, previously used by Sasaki and Kaiser in helichrome. Four copies of the 21-residue peptide $(LSLBLSL)_3$ (B = α-aminoisobutyric acid) were covalently linked through the peptide N-terminus to *meso*-tetrakis(*m*-carboxyphenyl)porphyrin via *m*-carboxamido linkages. *Meta* substitution provides optimal interhelical spacing for ion transport.

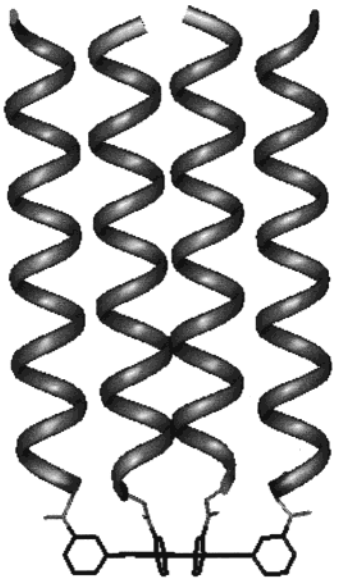

Figure 11. Molecular model of tetraphyillin.

A suitable strategy was applied for the synthesis of tetraphilins in order to overcome the major problems experienced in the synthesis of ion-channel-forming peptide, such as insolubility, tendency to aggregate, and microheterogeneity. To avoid these potential problems, eventually increased by the presence of the porphyrin, the complete assembly of the molecules by solid-phase methodology was not preferred. Therefore, the 21-residue peptide was first synthesized separately by the stepwise solid-phase method.[127] The purified, unprotected $(LSLBLSL)_3$ peptide was then coupled to the porphyrin moiety in solution to afford tetraphilin 1. The peptide−porphyrin conjugate tetraphilin 1 forms ion channels when incorporated into diphytanoyl phosphatidylcholine bilayers with a major conductance state (in 1 M HCl) of 470 pS indicative of a single molecular species with molecular dimensions envisioned in the model. As with the unlinked $(LSLBLSL)_3$ channel, the tetraphilin channels are proton-selective. Further, the lifetime of the major conductance state of the porphyrin-constrained tetraphilin (5 ms) is considerably longer than that of the unconstrained $(LSLBLSL)_3$ peptide (<0.2 ms). This property seems to indicate that the attachment of the peptide to the template stabilizes the conducting four-helix bundle state of the peptide. All the results obtained indicated that the porphyrin template exerts a major influence on the properties of $(LSLBLSL)_3$ channels by stabilizing the helical bundle in a stable, transmembrane configuration.

Nishino, Mihara, and co-workers also employed a similar strategy in the design and synthesis of an

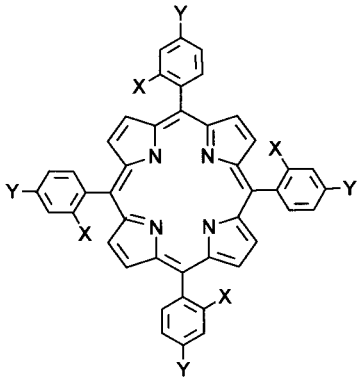

22-peptide: Ala-(Ala-Leu-Leu-Glu-Leu-Leu-Ala)$_3$-NHCH$_3$

Derivative	X	Y
orto-hybrid	CO-22-peptide	H
para-hybrid	H	CO-22-peptide

Figure 12. Schematic representation of the *ortho*- and *para*-hybrid derivatives, obtained by covalent linkage of the 22-peptide to the *meso*-tetrakis(carboxyphenyl)porphyrin, either in the *ortho* or *para* positions.

artificial four-helix bundle protein able to penetrate into membranes.[128,129] Four identical amphiphilic 22-residue peptides were N-terminally linked to *meso*-tetrakis(carboxyphenyl)porphyrin either in the *ortho* or *para* positions. The α,α,α,α-atropoisomer was preferred in the case of the *ortho* substitution (Figure 12).

The 21-residue peptide sequence (2−22) was synthesized, similarly to tetraphilin peptides, by condensation of 7-residue fragments assembled on oxime resin. The two hybrid proteins were obtained by coupling the protected 21-residue peptide with the *para* or α,α,α,α-*ortho* porphyrin-(Ala-OH)$_4$ derivatives. Side chain deprotection and purification by gel filtration afforded the two desired compounds, which showed different structural features and membrane-penetrating capacity. The *ortho*- and *para*-hybrids were characterized by CD spectroscopy in different media (CH_3OH, SDS micelle at pH 7.5, and DPPC vesicles at pH 7.5). First of all, the hybrids showed, in all the examined solvent systems, a CD-induced Cotton effect in the Soret region of opposite sign. This can be related to a different arrangement of the peptide chains with respect to the porphyrin ring. In the UV region, the CD spectra indicate a complete α-helical structure in CH_3OH solution for both the hybrids; the porphyrin template enhances the helical content as the peptide itself was only 50% helical. Further, the *ortho*-hybrid displayed a concentration-independent CD spectra, indicative of a monomeric structure: the linkage of the peptides to the porphyrin template in the *ortho* positions of the α,α,α,α-atropoisomer efficiently gather the peptides into the desired monomeric parallel four-helix bundle. In contrast, the concentration-dependent CD spectra observed for the *para*-hybrid is indicative of intermolecular helix−helix interactions: linkage to the *para* positions results in a molecule that is unable to fold intramolecularly. In SDS micelle and DPPC vesicles the *ortho*-hybrid is still highly helical (87%)

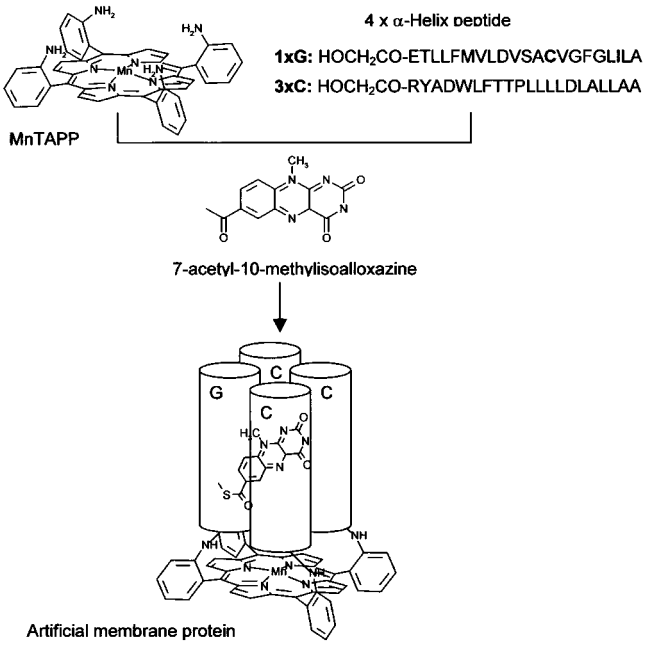

Figure 13. Artificial membrane protein functionalized with an electron trasfer system. C and G helices from bacteriorhodopsin were C-terminally linked to the *meso*-tetrakis(aminophenyl)porphyrin. In the G helix the Cys residue that bears the flavin cofactor is depicted in bold. (Adapted from ref 129.)

while the helicity of the *para*-hybrid is lowered (50% in SDS and 35% in DPPC). This finding indicates that the *ortho*-hybrid is capable of penetrating lipid bilayers without significant structural perturbation. Finally, gel filtration experiments confirmed that the *ortho*-hybrid was stably embedded into phospholipid bilayers whereas the *para*-hybrid was not. All the results obtained show that the rigid anchoring of the peptide chains to the porphyrin template in the *ortho*-hybrid strongly constrains the bundle structure. This rigidity is expected to forbid the perturbation of lipid bilayers and to stably embed the molecule into membranes. Further, the rigidity of the scaffold can also allow substitutions in the peptide sequence to engineer recognition sites inside the bundle. In a subsequent paper, the same authors reported the development of an artificial membrane protein functionalized with an electron-transfer system.[129] This protein is based on the previously employed α,α,α,α-atropoisomer of *meso*-tetrakis(2-carboxyphenyl)porphyrin, which acts as a template for assembling four peptide chains on one side of the porphyrin plane into a four-helix bundle motif. The four peptide sequences were taken from the C- and G-helices of the transmembrane regions of bacteriorhodopsin.[130] Mn(III) was inserted into the porphyrin ring, and a flavin cofactor was covalently linked to the side chain of a Cys residue in the G helix (Figure 13).

The presence of two coupled redox centers should allow the final protein to function as an electron-transfer system. The protein exhibits a high helical structure and was stably embedded into egg-yolk lecithin. The function as an electron-transfer path was examined using the protein embedded lecithin vesicles. Interestingly, the rate of Mn(III) reduction by dihydronicotinamide derivatives is accelerated by

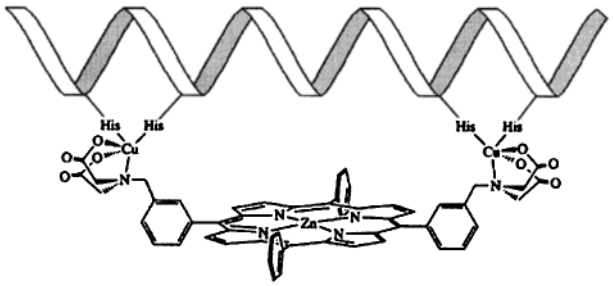

Figure 14. Molecular model of the helical-peptide-strapped zinc porphyrin. The sequences of the two peptides used in the development of the assembly are also indicated. (Reprinted with permission from ref 132. Copyright 1997 American Chemical Society.)

the presence of the covalently linked flavin moiety. This demonstrates that the two chromophores in the protein are well organized to promote electron transfer.

The porphyrin ring has also been employed for enhancing the α-helical folding in single peptide sequences. In particular, the design and synthesis of porphyrin-spanning peptides have been described;[131,132] the peptide is either covalently attached to *meso-tetra*-phenylporphyrin via *meta*-linkage on the phenyl rings or bound via metal-to-ligand coordination. Within the first class, Geier and Sasaki developed a peptide−porphyrin system made up of a 14-residue amphiphilic peptide containing two Cys residues at positions 2 and 13 of the sequence.[131] The Cys residues were inserted into the sequence for anchoring the peptide to the porphyrin via thioether linkage. CD spectra revealed that the helical content of the peptide increases up to 70% with increased TFE concentration (from 10% to 15%). Further, a larger induced Cotton effect in the Soret region was observed whose intensity decreases at increased TFE percentages. This behavior suggests that porphyrin aggregation occurs at low concentrations of the organic solvent. Finally, ^{1}H NMR spectra of both the conjugates and the peptide revealed that the peptide is positioned in proximity of the porphyrin ring as designed; in fact, the chemical shifts of the residues lying over the porphyrin ring are shifted upfield due to the porphyrin ring current.

Karpishin and co-workers reported a quite similar peptide−porphyrin assembly which incorporates a helical peptide strapped over a zinc−porphyrin.[132] This assembly is not driven by the coordination of a peptide side chain to the porphyrin metal center. The coordination of two copper ions by two pairs of His residues (positions 4−8 and 15−19) and two tridentate ligands, supported by the porphyrin ring, mediates the peptide−porphyrin assembly (Figure 14).

A 1:1 peptide−porphyrin stoichiometry was determined from amino acid analysis and flame atomic absorption spectroscopy; a spectrophotometric tritation also indicated a 1:1 binding stoichiometry. Further, size exclusion chromatography and electrospray mass spectrometry confirmed the monomeric nature of the assembly. EPR analysis indicates a N_3O_2 copper coordination. A high degree of helical structure in the peptide was found by CD spectroscopy, in agreement with the designed structure. The conformational stability of this system should enable modifications in the peptide sequence in order to engineer catalytic sites.

In summary, all systems herein described are excellent examples of using a porphyrin template to direct the folding of peptides into a helical conformation. This represents a promising technique, especially when applied to four-helix bundles. In fact, the stabilization of such a structure, with a unique aggregation state, will better allow one to study the effect of amino acid substitution on function as well the construction of defined functionality into the interior of the bundle.

III. Noncovalent Peptide–Porphyrin Systems

A remarkable feature of most heme−proteins is that the protoheme is tightly bound to the protein matrix, although, with the exceptions of the cytochrome *c* heme, it is not attached by covalent bonds. A large number of hydrophobic interactions and one or two coordinative bonds account for the high stability of the protoheme−protein complex.

Noncovalent peptide-porphyrin model systems are excellent candidates to rationalize all interactions that contribute to the structural stability of natural heme−proteins. The design strategy for the development of these systems is very challenging because it requires two sets of factors be taken into account simultaneously: (1) the construction of an artificial protein that adopts the unique desired folding and (2) the engineering into the interior of the designed protein of a proper cavity able to accommodate the large hydrophobic heme cofactor. A properly folded protein reduces the entropy loss that occurs when the protein interacts with the cofactor, as compared with flexible peptide chains. A favorable thermodynamic balance between the entropy loss, derived from the complex formation, and the enthalpy gain, derived from favorable interactions between the protein and the cofactor, accounts for a tight binding.

In recent years numerous very elegant papers have been published which report the development of noncovalent artificial heme−proteins. These novel model systems are mainly based on α-helical peptides able to self-assemble with the heme group. An important class of noncovalent heme−protein models is based on the four-helix bundle motif,[133] a ubiquitous and functionally important architecture found in many natural metalloproteins, such as cytochrome *c′* and cytochrome b_{562}.[134−136] The four-helix bundle motif can be classified on the basis of geometrical and topological properties. The helices in the bundle may adopt either parallel or antiparallel orientations.[133,137,138] A single-chain four-helix bundle with short connecting loops (such as in cytochrome b_{562})[136] exhibits an up−down−up−down arrangement which

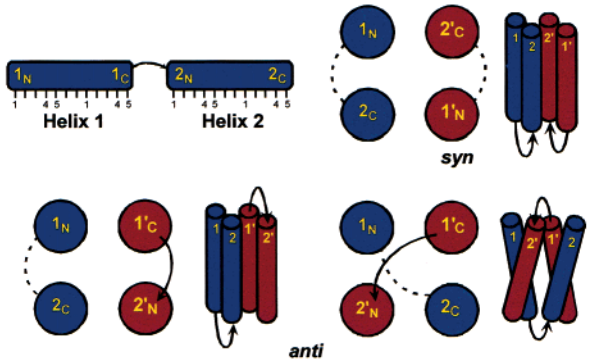

Figure 15. Different topologies adopted by right-handed homodimeric four-helix bundles. Left-handed helical bundles are also possible and have different interfacial interactions with respect to their right-handed correlates. (Reprinted with permission from ref 138. Copyright 2000 American Chemical Society.)

can come in two topologies, clockwise or counterclockwise turning. Longer loops may generate an up−down−down−up (such as in the ferritin family)[139] or an up−up−down−down (such as in the hematopoietic cytokine family)[139,140] connectivity. Dimeric four-helix bundles, which occur in nature in the form of noncovalently self-assembled proteins, such as ROP,[141] have a large number of possible topologies. A homodimeric four-helix bundle has six possible topologies (see Figure 15): four topologies have clockwise or counterclockwise turning loops that connect neighboring helices on either the same or opposite sides of the bundle.[142] Alternatively the loops can cross diagonally over the tops of the bundle in a motif first described in α2D and denoted the bisecting U.[143]

These considerations suggest that in designing four-helix bundles it is important to consider all possible folding topologies. The success of the design requires stabilization of the desired topology while destabilizing all other possible topologies. The structural characterization of both naturally occurring and designed four-helix bundles has shed light on the rules that govern this fold, and considerable progress has been made in the construction of a stable four-helix bundle with a unique topology.

Numerous excellent articles have appeared in the literature, and the reader may refer to these for recent advances in the field.[133,137,138,142−147]

Along these lines, the de novo protein design,[49−59] using minimalist[148−151] or binary patterning approaches,[152−155] has allowed the construction of stable four-helix bundles which were successfully used for the engineering of artificial heme−proteins with increasing complexity.

In this section we will survey the current state of the art of these artificial proteins, starting from simpler *mono*-heme peptide adducts. These systems were analyzed in an attempt to rationalize the interactions between heme and the protein and were also assayed for their functionality. Complex architectures encompassing more than one heme group or one heme coupled to a different cofactor, such as iron−sulfur cluster or flavin, will then be reviewed. In these systems the presence of multiple redox-active centers allowed the analysis of electron-transfer pathways.

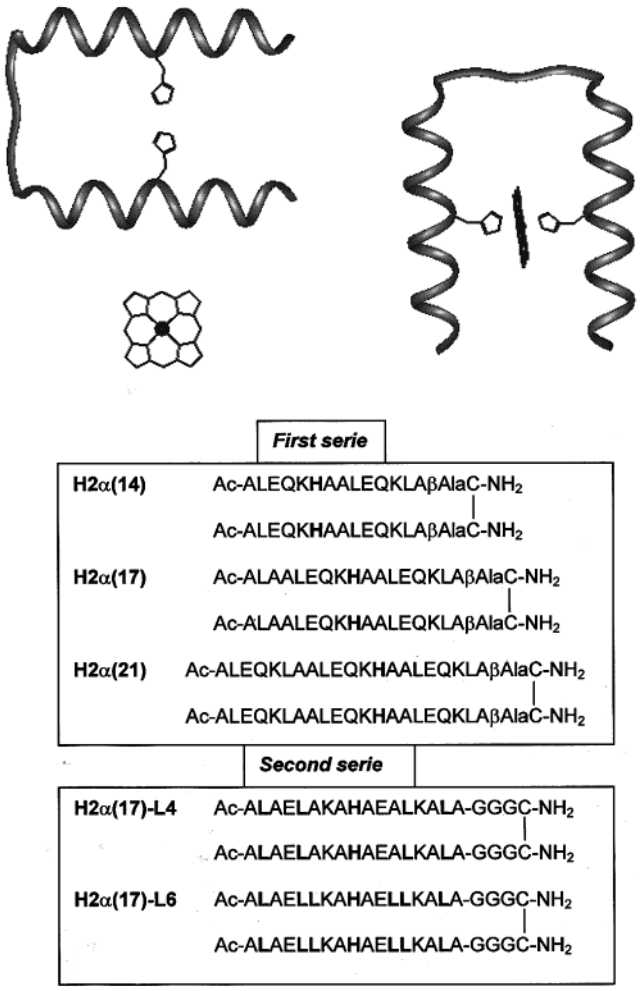

Figure 16. *Mono*-heme−peptide adducts developed by Mihara and co-workers. The peptide sequences of the first and second series are also indicated.

A. *Mono*-heme–Peptide Adducts

The molecular assembly of a single heme and peptides by noncovalent interactions has been deeply investigated by Mihara and co-workers.[156−163] A series of *mono*-heme peptide adducts have been developed by the design of two α-helical peptides, which are able to bind the heme group (Figure 16). These complexes have three main features: (1) the peptides were designed to assume an amphiphilic α-helix conformation, (2) two peptide segments were dimerized by disulfide linkage in order to have a structure consisting of two parallel α-helices, and (3) His residues were placed in the central position of each peptide sequence to coordinate the iron heme. The interaction between peptides and heme is driven by the formation of two coordinative Fe−His bonds and by the presence of a large number of hydrophobic residues, arranged around the His, to construct a hydrophobic heme-binding site.

At the first stage three peptides, H2α(14), H2α(17), and H2α(21) (Figure 16), of different chain lengths and containing a different number of Leu residues were designed.[156−158] The three peptide segments were designed on the basis of the coiled-coil heptad repeat[164] $(abcdefg)_n$, with hydrophobic residues Leu at the *a* and *d* positions, the hydrophilic Gln residues

Table 4. Relative Hydrophobicity, Binding Constant, and Initial Rates of Tetraguiacol Formation of Peptides H2α17-XY, Corresponding to the Following Schematic Formula

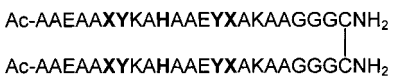

derivative	X	Y	relative hydrophobicity[a]	binding constant (10^7 M^{-1})[b]	initial rate ($10^6 M^{-1}$ min^{-1})[c]
H2α17-FF	Phe	Phe	5.00	4.7	0.49
H2α17-LF	Leu	Phe	4.99	1.9	0.56
H2α17-FL	Phe	Leu	4.85	3.4	0.36
H2α17-IL	Ile	Leu	4.31	1.2	0.30
H2α17-II	Ile	Ile	4.08	1.0	0.15
H2α17-LL	Leu	Leu	4.00	1.1	0.68
H2α17-LI	Leu	Ile	3.84	0.9	0.42
H2α17-VL	Val	Leu	2.51	0.5	2.12
H2α17-LV	Leu	Val	1.97	0.3	4.66
H2α17-VV	Val	Val	−0.12	not detectable	4.39
H2α17-LA	Leu	Ala	−0.60	not detectable	5.2
H2α17-AL	Ala	Leu	−0.99	not detectable	5.4
H2α17-AA	Ala	Ala	−5.00	not detectable	5.1

[a] Relative hydrophobicity of each peptide at the heme-binding site was estimated by the HPLC retention time (min). The experimentally measured retention times were converted to a relative hydrophobicity index for the corresponding X and Y residue pairs by using the following equation: $H = 10 \times \Delta t_{RXY-AA}/\Delta t_{RFF-AA} - 5.00$, where Δt_{RXY-AA} is the retention time difference between the peptide H2α17-XY and the most hydrophilic H2α17-AA and Δt_{RFF-AA} is the retention time difference between H2α17-FF and H2α17-AA. [b] The binding constants were determined from the absorbance change at the Soret band, using a single-site binding equation. [c] Initial rates for tetraguaicol formation were determined from spectrophotometric measurements (adapted from ref 159).

at the *f* position, ion-pair-forming residues Glu and Lys at the *e* and *g* positions, respectively, and Ala at the *b* and *c* positions. The two segments were dimerized by the disulfide linkage of Cys residues at the C-terminus. The His-coordinating residue was introduced at the *a* position, 6, 9, and 14 of H2α(14), H2α(17), and H2α(21), respectively.

Unfortunately, the analysis of these three peptides revealed that they had some structural insufficiency for a fixed haem binding. In fact, they showed a strong dependence on TFE concentration for accomplishing heme binding. For example, the peptides H2α(14) and H2α(17) were found to bind the heme only when the 2α-helix conformation was annealed by the addition of TFE. The peptide H2α(21), even though it showed a high helical content in buffer, was not able to bind heme without addition of TFE. In this case, TFE disrupts the tight interaction between the two helices, thus allowing the heme binding. These results showed that the peptide conformation, the rigidity of the helix−helix interaction at the heme-binding site, and the topology of the His residues are important for effective heme binding.

Further refinement of the design led to the development of a second series of peptides, based on an amphiphilic α-helix.[158] The main difference among the first and the second series was that in the latter the arrangements of the hydrophobic Leu residues were not ordered by the heptad rule of the coiled-coil motif (Figure 16). The improvement of the design in these new peptides was successful, since they all were found to adopt an α-helix structure in buffer solution and to bind the heme group with high affinities. These results demonstrated that the number and arrangement of Leu residues forming the heme-binding site in the α_2 structure were important in determining strong heme binding and fixing abilities to the peptide.

Interestingly, in these molecules a high binding affinity did not correspond to a high catalytic property.[158] The initial rate of the heme peroxidase activity in the oxidation of *o*-methoxyphenol to its tetramer *tetra*-guaiacol was measured in the presence and absence of the peptides. The designed peptides showed different behaviors in the modulation of the heme reactivity: it was significantly depressed by peptides that tightly bound to heme. This finding further confirmed, as found in natural *b*-type heme−proteins, that a tight packing of the protein environment around the heme together with the *bis*-His coordination strongly prevent the heme from reacting with an exogenous ligand.

To systematically evaluate the effect of amino acid substitutions on the heme-binding properties of the designed peptides, several derivatives were prepared (see Table 4).[159] In particular, by using the template peptide H2α17-LL, the series of peptides H2α17-XY was generated, in which residues X are at positions 5 and 13 and residues Y are at positions 6 and 12. To probe hydrophobic and steric interactions at the binding site, Phe, Ile, Val, Leu, and Ala were used as residues X and Y. A good correlation between peptide hydrophobicity and binding ability was found, thus demonstrating that the hydrophobic forces mainly stabilized the heme−peptide interaction (Table 4). Concerning the catalytic behaviors of the heme−peptide complexes, the trend previously observed was also found: a looser heme binding was reflected in a higher activity.

A striking feature was observed when positions 5, 6, 12, and 13 of H2α17-LL were substituted by the same residue, giving rise to H2α17-XX peptides, where Ile or Val are X residue.[160] Due to the conformational preferences of Ile and Val, it was expected that a *β*-strand rather than an α-helix structure would be stabilized. These two peptides showed a

helical conformation in absolute TFE, while the β-strand was observed in aqueous buffer. Further, the addition of heme to the peptide H2α17-II, in aqueous buffer, caused a structural transition from β-strand to α-helix. This peptide thus showed the unique property that its folding state was controlled by heme binding. This finding clearly highlighted the role of the heme cofactor as a structural element in artificial heme−peptide conjugates.

In an independent contribution, Suslick and co-workers also highlighted the reciprocal influence of peptides on the heme properties as well as that of the heme on the peptide properties.[165] These authors reported the analysis of 15-mer peptides possessing a palindromic sequence symmetry about the central His ligating residue. The peptides were designed in order to achieve helix formation and good water solubility, and they contain different amino acid (Phe, Leu, Nva, Ala, Aib, and Ser) to probe the influence of hydrophobic interactions on heme properties. The peptides were shown to bind Fe(III)−coproporphyrin I in a 2:1 stoichiometry, as designed, and they all experience a large increase in helicity upon heme binding. Interestingly, the heme peptide-binding constants span a range of almost 6000-fold relative to His (from 0.0081 $mmol^{-2}$ when His is the ligand to 47 $nmol^{-2}$ for the most tightly bound sequence). Hydrophobic interactions between the amphiphilic α-helices with the hydrophobic heme surface provide a good explanation for these large variations in binding. In fact, a strong correlation between side chain hydrophobicity and free energy of ligation was observed, thus confirming the importance of the hydrophobic effect in metalloporphyrin peptide complex stability. The reduction potential of the heme−peptide complexes correlates well with the binding constant values. A tighter binding is reflected in a decrease of reduction potentials, due to the higher preferences of Fe(III) to bind imidazole, with respect to Fe(II). On the other hand, the increase in peptide hydrophobicity should tend to stabilize Fe(II) over Fe(III); therefore, the observed trend in the reduction potential is somehow lessened by increased hydrophobicity. This is a clear example that multiple factors contribute to redox potentials in heme−proteins: the nature of the axial ligand and hydrophobicity both play an important role.

A series of disulfide bond-stabilized two-helix peptides was also designed by Benson and co-workers.[166] The peptides self-assemble with Co(III)−coproporphyrin or Co(III)−octaethylporphyrin to give *bis*-His-ligated complexes. As in the PSM molecules, reported by the same investigators, in which the heme is covalently linked to the peptide chains (see section II.D), also in this case helix induction arises upon metal−ligand coordination.

Mihara and co-workers also used a quite different approach to investigate the molecular basis in heme−peptide interactions.[162,163] The antigen-binding site of an antiheme monoclonal antibody was used to develop peptide sequences which could bind the porphyrin moiety. The amino acid sequence of the heavy chain of the complementarity determining region CDR-2 (CDRH-2) of the antiheme monoclonal antibody 2H5 was selected as starting template for peptide design. Even though no structural data were available for this peptide region, the conformation of the CDRH-2 was modeled as a β-strand−turn−β-strand, the structural motif commonly found in the CDRH-2 region of several antibodies showing a high degree of sequence similarity with 2H5. A set of peptides were thus designed with the aim of finding the minimal sequences able to bind the porphyrin, starting from the 20-mer natural sequence CRIDPANGNTKYDPKFQGKA. To provide structural stability to the model peptides, an intramolecular disulfide bridge, as conformational constraint, was inserted at various positions of the sequence. In addition, at the N-terminus a pyrene moiety was linked as a fluorescence probe to evaluate porphyrin binding. The minimal peptide sequence that retained high ability toward porphyrin binding was named 12C4, Py-GRI*C*PANG*C*TKY−NH_2.

To reveal the critical factors that determine the binding, the free peptide was extensively characterized by NMR spectroscopy. The chemical shift deviation together with the presence of NOEs between nonsequential residues strongly supported the peptide to adopt a packed structure rather than an extended β-strand. MD calculations, using all the NMR data, confirmed that the peptide adopted a bent structure. Porphyrin-binding studies by NMR spectroscopy allowed the authors to hypothesize that Ile, Arg, Lys, and pyrene moiety were strongly involved in the binding. All the information allowed carrying out a redesign procedure, which led to the further minimized peptide 9L. It corresponds to the PyGRINPGTKY−NH_2 sequence, in which the disulfide bridge was substituted by the turn Asn-Pro-Gly-Thr. By systematic amino acid replacement, peptides with improved affinity were obtained. This work has demonstrated the feasibility of using template structures to engineer functional peptides with binding ability toward several molecules and cofactors.

Another useful strategy for obtaining heme−protein models employs de novo designed four-helix bundle scaffolds in which interior heme-binding sites can be engineered. Dutton, DeGrado, and co-workers described a number of four-helix bundle proteins that spontaneously fold in aqueous solution and assemble with one or more hemes.[167−182] Initial work focused on two derivatives of the dimeric α_2B four-helix bundle,[183] named $VAVH_{25}$(S−S) and retro(S−S), made up of two helix−loop−helix peptides, N-terminally linked through a disulfide bridge (Figure 17).[167] Retro(S−S) is a variant of $VAVH_{25}$(S−S) with a reversed peptide sequence.

The sequences were carefully engineered to create in the interior of the bundle a hydrophobic cavity to accommodate a single low-spin *bis*-histidine-ligated heme. The design successfully resulted in the construction of four-helix bundles able to bind the heme in the desired cavity with a 1:1 stoichiometry. Experimental evidences for a *bis*-histidine ligation were found for both complexes, even though comparable amounts of low- and high-spin ferric−hemes were present in $VAVH_{25}$(S−S) while a low-spin ferric−heme predominated in retro(S−S). Further, different

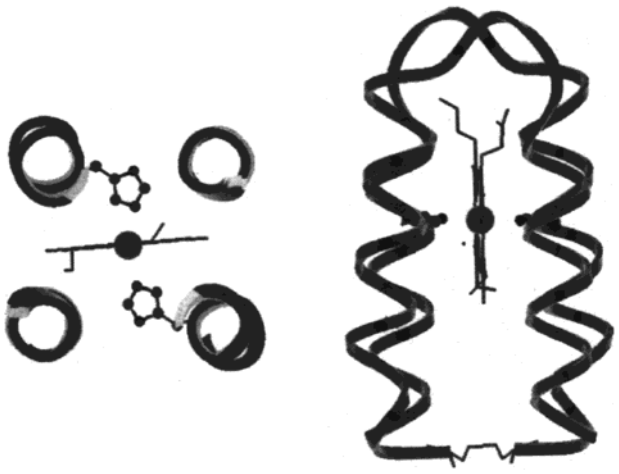

Figure 17. Molecular model of the retro(S−S) peptide with bound heme. (Left) View looking down the core of the bundle at the heme-binding site. (Right) Lateral view of the protein model, with the loop positioned at the top and the disulfide positioned at the bottom of the bundle. (Adapted from ref 167.)

dissociation constants (in the micromolar to nanomolar range) were found for the two proteins. Interestingly, the less tightly bound $VAVH_{25}$(S−S) is fully folded in both the *apo* and *holo* forms whereas the tighter coordinating retro(S−S) is only partially folded in the absence of heme. The redox midpoints (−170 and −220 mV for $VAVH_{25}$(S−S) and retro(S−S), respectively) and the fairly low fluorescence intensity of the Zn−protoporphyrin derivative suggested that the heme is more accessible to solvent than originally anticipated. All these results suggest that an accurate control of the heme ligation is not easy to accomplish and requires specific features in order to improve the affinity of binding. For example, a small degree of flexibility can be advantageous in designed heme−proteins as it can allow searching for the best coordinating conformation.

B. *Multi*-heme– and Heme-Cofactor–Peptide Adducts

Numerous redox proteins and oxidoreductase enzymes accomplish their functions using more than one equal or different cofactor. The design of artificial proteins that assemble in a well-defined three-dimensional structure and able to accommodate more than one cofactor in their interior is very ambitious, since the designed framework should specifically bind the cofactors with high affinity and in the correct positions.

Dutton and co-workers reached impressive results in the design of minimalist protein structures, called molecular *maquettes*, which assemble arrays of cofactors and reproduce nativelike functions. They developed a series of model heme−proteins containing multiple redox-active centers capable of electron transfer.[168−182]

These compounds were constructed on the basis of B and D helices of cytochrome bc_1,[184,185] and the basic building block is an α_2 motif, intended to dimerize into a four-helix bundle. The prototype is made up of a 62-residue parallel α_2 system in which two

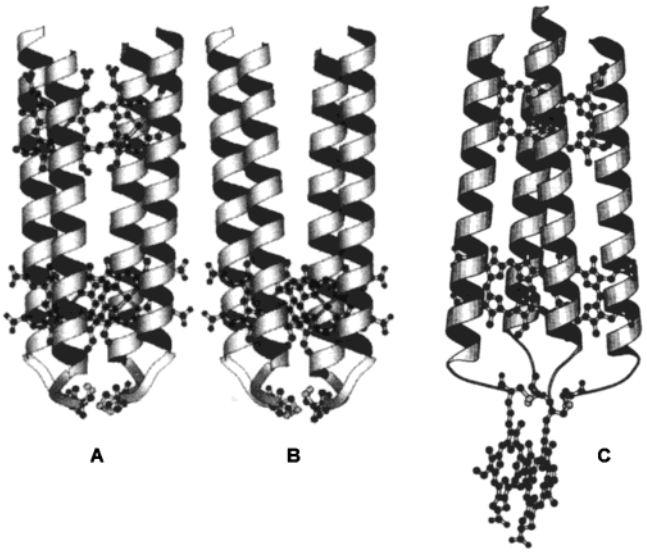

Figure 18. Molecular models of maquettes: (A) cytochrome *c* maquette; (B) maquette variant containing only one couple of heme at the 10,10′ positions; (C) coproporphyrin-linked maquette. (Reprinted with permission from refs 169 and 174. Copyright 1997 American Chemical Society.)

identical helices are linked by a disulfide bridge in a parallel orientation (α-SS-α).[168] The α_2 dimer was designed to associate into a parallel four-helix bundle. Each α_2 dimer contains two pairs of histidines, in positions 10, 10′ and 24, 24′, and was intended to bind two hemes; thus, the complete four-helix assembly should result in four *bis*-His-ligated hemes. A schematic representation of this synthetic cytochrome *b* maquette is presented in Figure 18A. The spectral, electrochemical, and heme binding properties of this heme−maquette closely resemble those of native proteins and are fully consistent with the working model for its structure.

The heme binding was demonstrated to be specific and dependent on the His ligation; in fact, variants lacking one histidine pair (10,10′ or 24,24′) were shown to bind only two hemes *per* four-helix bundle.[168] Redox titration of the cytochrome *b* maquette indicated that the electrochemical properties of the four hemes are markedly different; despite the 2-fold axis of symmetry bewteen the two α_2-subunits, also the two pairs of hemes ligated in 10,10′ and 24,24′ showed different redox potential. To ascertain whether these differences arise from electronic interactions between the hemes or from different protein environments experienced by each heme, a simpler maquette containing only one couple of heme, at 10,10′ positions (see Figure 18B), was studied in detail.[169] In particular, RR studies, using a number of different hemes, indicated that the two hemes are structurally identical, and therefore, their redox inequivalence is due to heme−heme interactions. In addition, using both the entire cytochrome *b* maquette and the simpler H10,10′ maquette, the same investigators reported that heme redox potential can be modulated by changes in heme peripheral substitution, charge distribution in heme proximity, and protonation state of the neighboring amino acids;[170−172] further, the heme-binding affinity is strongly related to the posi-

tion of the coordinating residues within the heptad repeat.[173]

Even though these maquettes were shown to have a high degree of helical content, both the *apo*-peptides and the heme complexes showed dynamic behavior that precluded their structure determination by NMR. However, the supposed all-parallel structure was supported by a subsequent work in which a covalently linked coproporphyrin α_2 was shown to form a cofacial dimer in the four-helix bundle (see Figure 18C).[174]

To improve the properties of the prototype and to obtain functional molecules with more nativelike structures, a series of parallel and antiparallel heme-binding four-helix bundles were synthesized.[175−178] In the parallel variants, the effect of packing specificity was evaluated by substituting the leucine at positions 6 and 13 of the prototype sequence[168] with β-branched and or aromatic amino acids.[175] All variants bind heme similarly to the prototype and showed enhanced stability. However, the heme-bound states of these proteins still have significant dynamic character, precluding structure determination by NMR. The *apo* state of the variants fold into a relatively unique structure,[175,176] and the most stable Leu6Ile, Leu13Phe variant was expressed in *E. coli* and structurally characterized by NMR spectroscopy. The structure confirmed many expected design features and supported the four-helix bundle quaternary structure $(\alpha\text{-SS-}\alpha)_2$. The main results can be summarized as follows. The two helices in the (α-SS-α) unit are not magnetically equivalent. The covalent α_2 unit forms a noncovalent dimer which contains a 2-fold symmetry axis as expected; however, the bundle can adopt both the *syn* and *anti* topology, as also confirmed by different spectroscopic evidences. Thus, the four-helix bundle possesses a nativelike interface between the covalent bound α-helices, while the adjacent noncovalent interface shows nonnativelike behaviors. Most important, the tight hydrophobic packing around the heme ligands His10,10′, His24,-24′ does not allow the formation of cavities where the hemes can be accommodated. This finding accounts for the observed lack of a unique structure in the heme-bound state of the designed protein. Nevertheless, the designed scaffold is sufficiently rigid to allow amino acid substitutions in order to improve the properties of the heme-ligated forms.

Alternative four-helix bundle topologies for maquette construction were also developed by converting the (α-SS-α) unit into a single polypeptide chain helix−loop−helix, intended for self-assembly into the dimeric four-helix bundle $(\alpha\text{-}l\text{-}\alpha)_2$.[177,178] Further construction of a disulfide bridge between two (α-*l*-α) monomers yields a 126-residue single-molecule four-helix bundle (α-*l*-α-SS-α-*l*-α).[178]

The feasibility of using the maquette architecture for the development of synthetic multi-cofactor redox proteins was also proved, and maquettes incorporating hemes with iron−sulfur clusters,[179] flavins,[180] and zinc−porphyrins[181] were synthesized.

A ferredoxin−heme maquette was developed by introducing an Fe_4S_4 cluster into the loop region of a helix−loop−helix peptide able to dimerize (Figure 19).[179] The helical regions were designed on the basis of the cytochrome *b* maquette,[168] which are able to bind four hemes with a *bis*-His ligation. A 16-residue peptide derived from the consensus motif of natural ferredoxins was inserted into the loop region.

The successful assembly of the protein cofactors was demonstrated by several spectroscopic techniques, even though the detailed overall structure remains to be established. Remarkable results were gained with maquette incorporating both the flavin cofactor and heme group. Photoreduction of the hemes was successfully demonstrated by electron transfer between light-activated flavins and the iron porphyrins.

All these outstanding results indicate that the maquettes constituted an excellent framework for the positioning of juxtaposed redox groups capable of performing long-range electron transfer. The possibility of modulating the metal redox potentials by subtle changes in the protein composition will allow one to design multi-cofactor synthetic proteins with predetermined properties.

To control the topology of artificial four-helix bundle proteins, the TASP approach[125] was employed by Haehnel and co-workers.[186,187] The first molecule, MOP1, able to bind hemes was engineered using four α-helical peptides covalently connected to a cyclic decapeptide template.[186] The helical segment design was based on the crystal structure of the cytochrome *b* subunit of the mitochondrial cytochrome bc_1 complex.[185] Two helices, H1 and H2, were designed in an attempt to reproduce the main features of the cytochrome *b* A−D helices. The H1 helix bears two His residues analogously to the B and D helices, while the H2 helix does not contain any coordinating residues and like A and C helices shields the heme-binding pocket against the solvent. Two H1 helices were covalently linked to the template in a parallel orientation and antiparallel to a parallel H2 helix couple. A suitable chemoselective synthetic strategy was developed in order to control the directionality of the helical segments. The spectroscopic properties of the bound heme revealed the successful assembly of the model heme−protein. Two midpoint redox potentials were found for the two hemes with values quite different from those previously reported in the model of DeGrado and Dutton[168] and close to those found for the two hemes in cytochrome *bf* complex.[188]

In a subsequent work, by assembling three different helices on a cyclic peptide template a multi-cofactor four-helix bundle system containing both a single heme and a ruthenium−tris(bipyridine) complex was developed.[187] Two derivatives MOP2 and MOP3 were synthesized, differing in the position of the ruthenium complex with respect to the heme group. In these systems, the heme group is bound in the hydrophobic interior via two His residues coming from helices H1 and H3 in MOP2 and H1 and H4 in MOP3. One of the heme-binding helices, H3 or H4, serves also as an attachment site for the ruthenium complex. A Cys residue on the hydrophilic side, at position 16 in H3 and position 13 in H4, allows selective thioether formation with the bromomethylated ruthenium complex. The spectroscopic charac-

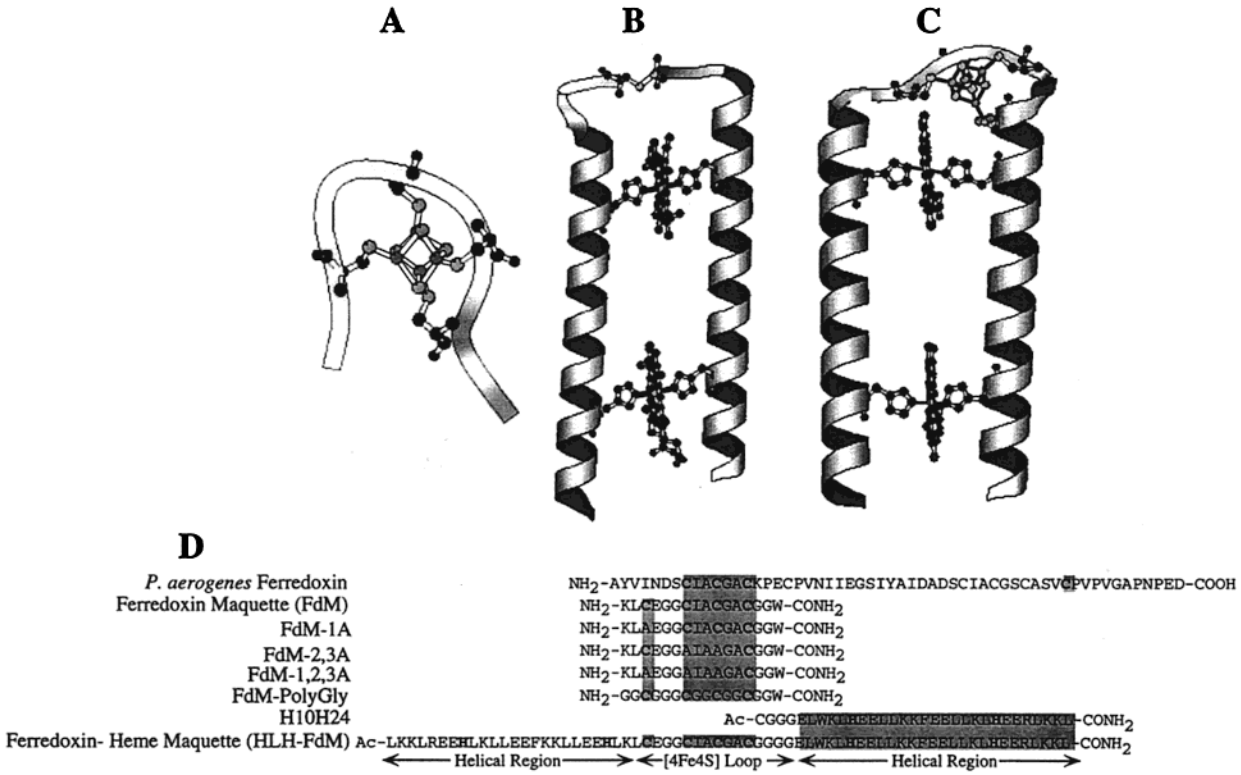

Figure 19. Modular design of the ferredoxin maquette. (A) MOLSCRIPT model of the monomeric hexadecapeptide with bound [4Fe-4S]. (B) Molecular model of the prototype heme−protein maquette H10H24. (C) Computer representation of the modular design helix−loop−helix ferredoxin−heme maquette (HLH−FdM) with a [4Fe-4S] cluster and a pair of bound hemes. (D) Primary sequence alignment illustrating the modular peptide design approach. Given are the sequences for *Peptococcus aerogenes* Fd (from which the [4Fe-4S]-binding domain was extracted), the natural sequence ferredoxin maquette FdM, versions of the ferredoxin maquette with one, two, and three cysteines to alanine modifications, the glycine-modified ferredoxin maquette, and the HLH−FdM. All synthetic peptides were C-terminally amidated, and the HLH−FdM was N-terminally acetylated. (Reprinted with permission from ref 179. Copyright 1996 National Academy of Science.)

terizations are consistent with the structure predetermined by the template. Laser-induced absorbance changes revealed that electron transfer, between the two cofactors occurs in both MOP2 and MOP3, even though further studies are needed in an attempt to simplify the electron-transfer kinetics.

Using their template-assisted system, the same authors generated a large collection of novel heme−proteins.[189] In particular, they reported the synthesis and characterization of a library of 462 proteins, derived from small libraries of peptide building blocks, which were attached to a template bound to a cellulose membrane. The peptide libraries were synthesized by variation of the residues, which were shown, by molecular modeling, to form the hydrophobic heme-binding pocket. Solid-phase spectroscopic characterization allowed selecting 399 proteins able to bind the heme, which were subsequently screened for the midpoint potential of the heme group. The combinatorial approach was successful in finding proteins that tune the heme midpoint potential from −90 to −150 mV. Further studies are needed in order to correlate the amino acid composition with the observed midpoint redox potentials. The most relevant aspect of this work is that the developed strategy can be applied for the synthesis of large numbers of receptor-like molecules, novel metalloproteins, and catalysts.

Hecht and co-workers used the binary patterning approach in the design of *semi*-random libraries of peptides, screened for their ability to bind heme.[154,190,191] Among 30 binary code sequences tested, 15 were shown to bind heme with a broad range of affinities and with spectroscopic features resembling those of natural cytochromes.[154] In a subsequent work, it was demonstrated that several of the "binary code" proteins possess peroxidase activity at rates rivaling natural peroxidases.[190] Eight "binary pattern" heme−proteins, derived from two combinatorial libraries, were also assessed for carbon monoxide binding.[191] The CO binding affinities for all proteins were similar to that of myoglobin,[191] with dissociation constants in the nanomolar range. RR studies indicated that none of the eight "binary code" proteins contribute a H-bond donor or a lone pair for interaction with the CO. Such interactions are often observed in the CO adducts of natural heme−proteins;[192] the lack of explicit design causes these "binary code" proteins unable to make specific directional interactions with bound ligands.

All these results are particularly encouraging because they suggest that "*semi*-random" libraries may produce artificial heme−proteins which may have catalytic and binding activities. Nevertheless, the construction of specific desired functionality within these artificial heme−protein requires explicit design, genetic selections, or both.

Very recently, peptide−porphyrin complexes have been used in the construction of supramolecular architectures, which resemble natural photosynthetic

systems.[193,194] To develop such an artificial system, dendrimers have been used as templates. Dendrimers are hyperbranched macromolecules with well-defined three-dimensional shapes containing a different number of end groups, which determines the packing. A multi-metalloporphyrin assembly, which resembles the natural light-harvesting antenna in photosynthetic bacteria, was constructed by combining dendrimers and de novo designed peptides. Amphiphilic 20-residue α-helices, containing a His ligand in the central position, were linked at the end groups (4, 8, 16, 32, or 64 segments) of polyamidoamine dendrimers. The peptide dendrimers were shown to bind Fe(III)− or Zn(II)−mesoporphyrin IX *per* two helices. CD studies suggested that metalloporphyrins were coordinated to the peptide−dendrimers in a regulated manner and packed more densely with the increase in the number of branched units. The enlargement of the dendrimer generation causes a decrease in the peroxidase-like activity and an increase in the electron-transfer efficiency. Thus, the construction of peptide−dendrimers constitutes an important approach in the development of artificial photosynthetic systems as well as of different functional macromolecules, such as catalysts and biosensors.

IV. Conclusions and Perspectives

The results reported in this review demonstrate the feasibility of constructing artificial heme−proteins. From the first attempts of Traylor to develop simple oxygen-carrier models, numerous and more elaborate heme−protein models have appeared in the literature. Synthetic peptides and proteins that bind the heme and assume a unique overall fold have been designed and extensively characterized, thus providing insights into the understanding of the structure−function relationships in heme−proteins. Most of the factors that tune the properties of the heme are well understood, and it is now clear that small differences in the packing, hydrophobicity, binding pocket flexibility, and ligand orientation can significantly influence the characteristics of natural and artificial heme−proteins. This has allowed developing novel and important heme−protein models which may find widespread practical applications. However, the functional specificity of the natural systems has not been completely achieved, and therefore, one of the most challenging directions in the near future is to reproduce in artificial molecules the subtle mechanisms that control the heme functions, thus ensuring the selectivity of the natural systems. This important goal may certainly be the result of an iterative process of design and rigorous characterization. Even in the case of unsuccess, a complete spectroscopic and structural characterization may allow one to diagnose the problems associated with the initial models and to improve the models in subsequent designs. Modern techniques of characterization and methods of combinatorial synthesis may help to more rapidly optimize the initial design. Further, the development of several rigid scaffolds able to stably accommodate the heme in their interior may easily allow introducing systematic variations into the sequence without perturbing the overall structure. Thus, the mechanism through which the peptide environment imparts selectivity to the heme can be investigated, finally leading to the construction of models able to stabilize the desired reactivity over many other possibilities.

V. List of Abbreviations

Abbreviations used for natural amino acids and peptides are according to the IUPAC−IUM Commission on Biochemical Nomenclature.

NMR	nuclear magnetic resonance
CD	circular dicroism
EPR	electron paramagnetic resonance
MP	microperoxidases
CTAB	cetyl trimethylammonium bromide
SDS	sodium dodecyl sulfate
Im	imidazole
Ac	Acetyl
ABTS	2,2′-azino-bis[3-ethylbenzthiazoline-6-sulfonic acid]
Fmoc	9-fluorenyl-methoxy-carbonyl
DMSO	dimethylsulfoxide
RP-HPLC	reverse phase high-performance liquid chromatography
RMD	restrained molecular dynamics
DPPC	dipalmitoylposphatidylcholine
PSM	peptide-sandwiched mesoheme
NADPH	nicotinamide adenine dinucleotide phosphate
TASP	template-assembled synthetic proteins
Hb	hemoglobin
Mb	myoglobin
P450−CAM	cytochrome P450 camphor-free
PrOH	1-propanol
TFE	2,2,2-trifluoroethanol
MD	molecular dynamics
NOE	nuclear Overhauser effect
RR	resonance Raman

VI. Acknowledgments

We thank W. F. DeGrado for critically reading the manuscript and many colleagues for providing us with reprints of their works. Our work was partly supported by the Italian Ministry of University and Scientific Research (PRIN 9803184222).

VII. References

(1) Lippard, S. J.; Berg, J. M. *Principles of Bioinorganic Chemistry*; University Science Books: Mill Valley, 1994; p 349.
(2) Holm, R. H.; Kennepohl, P.; Solomon, E. I. *Chem. Rev.* **1996**, *96*, 2239.
(3) *The Porphyrins*; Dolphin, D., Ed.; Academic Press: New York, 1979; Vol. 7.
(4) Bertini, I.; Luchinat, C. *Curr. Opin. Chem. Biol.* **1999**, *3*, 145.
(5) Perutz, M. F.; Wilkinson, A. J.; Paoli, M.; Dodson, G. G. *Annu. Rev. Biophys. Biomol. Struct.* **1998**, *27*, 1.
(6) Peterson, J. A.; Graham, S. E. *Structure* **1998**, *6*, 1079.
(7) Loew, G. H.; Harris, D. L. *Chem. Rev.* **2000**, *100*, 407.
(8) Li, H.; Poulos, T. L. *Structure* **1994**, *2*, 461.
(9) Wong, L. L. *Curr. Opin. Chem. Biol.* **1998**, *2*, 263.
(10) Smith, A. T.; Veitch, N. C. *Curr. Opin. Chem. Biol.* **1998**, *2*, 269.
(11) Banci, L. *J. Biotechnol.* **1997**, *53*, 253.
(12) Sono, M.; Roach, M. P.; Coulter, E. D.; Dawson, J. H. *Chem. Rev.* **1996**, *96*, 2841.
(13) Barker, P. D.; Ferguson, S. J. *Structure* **1999**, *7*, R281.
(14) Poulos, T. L.; Li, H.; Raman, C. S. *Curr. Opin. Chem. Biol.* **1999**, *3*, 131.
(15) Michel, H.; Behr, J.; Harrenga, A.; Kannt, A. *Annu. Rev. Biophys. Biomol. Struct.* **1998**, *27*, 329.
(16) Lederer, F. *Biochimie* **1994**, *76*, 674.
(17) Hellinga, H. W. *Protein Engineering: Principles and Practice*; Wiley-Lyss, Inc.: New York, 1996, p 369.
(18) Poulos, T. L. *J. Biol. Inorg. Chem.* **1996**, *1*, 356.

(19) Goodin, D. B. *J. Biol. Inorg. Chem.* **1996**, *1*, 360.
(20) Banci, L.; Rosato, A.; Turano, P. *J. Biol. Inorg. Chem.* **1996**, *1*, 364.
(21) Gross, Z. *J. Biol. Inorg. Chem.* **1996**, *1*, 368.
(22) Rietjens, I. M. C. M.; Osman, A. M.; Veeger, C.; Zakharieva, O.; Antony, J.; Grodzichi, M.; Trautwein, A. X. *J. Biol. Inorg. Chem.* **1996**, *1*, 372.
(23) Weiss, R.; Mandon, D.; Wolter, T.; Trautwein, A. X.; Muther, M.; Bill, E.; Gold, A.; Jayaraj, K.; Terner J. *J. Biol. Inorg. Chem.* **1996**, *1*, 377.
(24) Winkler, J. R.; Wittung-Stafshede, P.; Leckner, J.; Malmstrom, B. G.; Gray, H. B. *Proc. Natl. Acad. Sci.* **1997**, *94*, 4246.
(25) Adachi, S.; Nagano, S.; Ishimori, K.; Watanabe, Y.; Morishima, I.; Egawa, T.; Kitagawa, T.; Makino, R. *Biochemistry* **1993**, *32*, 241.
(26) Tezcan, F. A.; Winkler, J. R.; Gray, H. B. *J. Am. Chem. Soc.* **1998**, *120*, 13383.
(27) Mauk, A. G.; Moore, G. R. *J. Biol. Inorg. Chem.* **1997**, *2*, 119.
(28) Gunner, M. R.; Alexov, E.; Torres, E.; Lipovaca, S. *J. Biol. Inorg. Chem.* **1997**, *2*, 126.
(29) Naray-Szabo′, G. *J. Biol. Inorg. Chem.* **1997**, *2*, 135.
(30) Wuttke, D. S.; Gray, H. B. *Curr. Opin. Struct. Biol.* **1993**, *3*, 555.
(31) Gray, H. B.; Winkler, J. R. *Annu. Rev. Biochem.* **1996**, *65*, 537.
(32) Nastri, F.; Lombardi, A.; D′Andrea, L. D.; Sanseverino M.; Maglio, O.; Pavone, V. *Biopolymers* **1998**, *47*, 5.
(33) Traylor, T. G. *Acc. Chem. Res.* **1981**, *14*, 102.
(34) Traylor, T. G.; Chang, C. K.; Geibel, J.; Berzinis, A.; Mincey, T.; Cannon, J. *J. Am. Chem. Soc.* **1979**, *101*, 6716.
(35) Collman, J. P. *Inorg. Chem.* **1997**, *36*, 5145.
(36) Momenteau, M.; Reed, C. A. *Chem. Rev.* **1994**, *94*, 659.
(37) Mansuy, D.; Battioni, P. *Bioinorganic Catalysis*; Marcel Dekker: New York, 1993; p 395.
(38) Mansuy, D. *Coord. Chem. Rev.* **1993**, *125*, 129.
(39) Meunier, B. *Chem. Rev.* **1992**, *92*, 1411.
(40) Collman, J. P.; Zhang, X.; Lee, V. J.; Uffelman, E. S.; Brauman, J. I. *Science* **1993**, *261*, 1404.
(41) Karlin, K. D. *Science* **1993,** *261*, 701.
(42) Liang, H. C.; Dahan, M.; Karlin, K. D. *Curr. Opin. Chem. Biol.* **1999**, *3*, 168.
(43) Ibers, J. A.; Holm, R. H. *Science* **1980**, *209*, 223.
(44) Hellinga, H. W. *Curr. Opin. Biotechnol.* **1996**, *7*, 437.
(45) Hellinga, H. W. *Folding Des.* **1998**, *3*, R1.
(46) DeGrado, W. F.; Summa, C. M.; Pavone, V.; Nastri, F.; Lombardi, A. *Annu. Rev. Biochem.* **1999**, *68*, 779.
(47) Regan, L. *Trends Biochem. Sci.* **1995**, *20*, 280.
(48) Lu, Y.; Valentine, J. S. *Curr. Opin. Struct. Biol.* **1997**, *7*, 495.
(49) Baltzer, L. *Topics Curr. Chem.* **1999**, *202*, 39.
(50) Richardson, J. S.; Richardson, D. C.; Tweedy, N. B.; Gernert, K. M.; Quinn, T. P.; Hecht, M. H.; Erickson, B. W.; Yan, Y.; McClain, R. D.; Donlan, M. E.; et al. *Biophys. J.* **1992**, *63*, 1185.
(51) Bryson, J. W.; Betz, S. F.; Lu, H. S.; Suich, D. J.; Zhou, H. X.; O′Neil, K. T.; DeGrado, W. F. *Science* **1995**, *270*, 935.
(52) Betz, S. F.; Raleigh, D. P.; DeGrado, W. F. *Curr. Opin. Struct. Biol.* **1993**, *3*, 601.
(53) Beasley, J. R.; Hecht, M. H. *J. Biol. Chem.* **1997**, *272*, 2031.
(54) Balaram, P. *J. Pept. Res.* **1999**, *54*, 195.
(55) Imperiali, B.; Ottesen, J. J. *Biopolymers* **1998**, *47*, 23.
(56) Tuchscherer, G.; Scheibler, L.; Dumy, P.; Mutter, M. *Biopolymers* **1998**, *47*, 63.
(57) Street, A. G.; Mayo, S. L. *Structure* **1999**, *7*, R105.
(58) Desjarlais, J. R.; Handel, T. M. *Protein Sci.* **1995**, *4*, 2006.
(59) Desjarlais, J. R.; Clarke, N. D. *Curr. Opin. Struct. Biol.* **1998**, *8*, 471.
(60) Gouterman, M. *The Porphyrins*; Academic Press: New York, 1978; Vol. 3, p 1.
(61) Adar, F. *The Porphyrins*; Academic Press: New York, 1978; Vol. 3, p 167.
(62) Eaton, W. A.; Hofrichter, J. *Methods Enzymol.* **1981**, vol. 76, p 175.
(63) Buchler J. W. *The Porphyrins;* Academic Press.: New York, 1979; Vol. 1, p 389.
(64) Bullock, P. A.; Myer, Y. P. *Biochemistry* **1978**, *17*, 3084.
(65) Babcock, G. T.; Widger, W. R.; Cramer, W. A.; Oertling, W. A.; Metz, J. G. *Biochemistry* **1985**, *24*, 3638.
(66) Sugiyama, T.; Miura, R.; Yamano, T.; Shiga, K.; Watari, H. *Biochem. Biophys. Res. Commun.* **1980**, *97*, 22.
(67) Dawson, J. H.; Andersson, L. A.; Masanori, S. *J. Biol. Chem.* **1982**, *257*, 3606.
(68) Wang, J. H. *Oxygenases*; Academic Press: New York, 1962; p 502.
(69) Tuppy, H.; Paleus, S. *Acta Chem. Scand.* **1955**, *9*, 353.
(70) Paleus, S.; Ehrenberg, A.; Tuppy, H. *Acta Chem. Scand.* **1955**, *9*, 365.
(71) Aron, J.; Baldwin, D. A.; Marques, H. M.; Pratt, J. M.; Adams, P. A. *J. Inorg. Biochem.* **1986**, *27*, 227.
(72) Low, D. W.; Yang, G.; Winkler, J. R.; Gray, H. B. *J. Am. Chem. Soc.* **1997**, *119*, 4094.
(73) Ehrenberg, A.; Theorell, H. *Acta Chem. Scand.* **1955**, *9*, 1193.
(74) Urry, D. W. *J. Am. Chem. Soc.* **1967**, *89*, 4190.
(75) Urry, D. W.; Pettegrew, J. W. *J. Am. Chem. Soc.* **1967**, *89*, 5276.
(76) Sasaki, T.; Kaiser, E. T. *J. Am. Chem. Soc.* **1989**, *111*, 380.
(77) Sasaki, T.; Kaiser, E. T. *Biopolymers* **1990**, *29*, 79.
(78) Akerfeldt, K. S.; Kim, R. M.; Camac, D.; Groves, J. T.; Lear, J. D.; DeGrado, W. F. *J. Am. Chem. Soc.* **1992**, *114*, 9656.
(79) Benson, D. R.; Hart, B. R.; Zhu, X.; Doughty, M. B. *J. Am. Chem. Soc.* **1995**, *117*, 8502
(80) Othman, S.; Le Lirzin, A.; Desbois, A. *Biochemistry* **1994**, *33*, 3**,** 15437.
(81) Othman, S., Le Lirzin, A.; Desbois, A. *Biochemistry* **1993**, *32*, 9781.
(82) Mazumdar, S.; Medhi, O. K.; Mitra, S. *Inorg. Chem.* **1991**, *30*, 700.
(83) Wang, J. S.; Tsai, A. L.; Heldt, J.; Palmer, G.; Van Wart, H. E. *J. Biol. Chem.* **1992**, *267*, 15310.
(84) Munro, O. Q.; Marques, H. M. *Inorg. Chem.* **1996**, *35*, 3752.
(85) Munro, O. Q.; Marques, H. M. *Inorg. Chem.* **1996**, *35*, 3768
(86) Carraway, A. D.; McCollum, M. G.; Peterson, J. *Inorg. Chem.* **1996**, *35*, 6885.
(87) Adams, P. A.; Good, R. D. *J. Chem. Soc., Chem. Commun.* **1990**, 97.
(88) Adams, P. A. *J. Chem. Soc., Perkin Trans. 2* **1990**, 1407.
(89) Cunningham, I. D.; Bachelor, J. L.; Pratt, J. M. *J. Chem. Soc., Perkin Trans. 2* **1991**, 1839.
(90) Cunningham, I. D.; Snare, G. R. *J. Chem. Soc., Perkin Trans. 2* **1992**, 2019.
(91) Cunningham, I. D.; Bachelor, J. L.; Pratt, J. M. *J. Chem. Soc., Perkin Trans. 2* **1994**, 1347.
(92) Osman, A. M.; Koerts, J.; Boersma, M. G.; Boeren, S.; Veeger, C.; Rietjens, I. M. C. M. *Eur. J. Biochem.* **1996**, *240*, 232.
(93) Osman, A. M.; Boeren, S.; Boersma, M. G.; Veeger, C.; Rietjens, I. M. C. M. *Proc. Natl. Acad. Sci.* **1997**, *94*, 4295.
(94) Dorovska-Taran, V.; Posthumus, M. A.; Boeren, S.; Boersma, M. G.; Teunis, C. J.; Rietjens, I. M. C. M.; Veeger, C. *Eur. J. Biochem.* **1998**, *253*, 659.
(95) Primus, J. L.; Boersma, M. G.; Mandon, D.; Boeren, S.; Veeger, C.; Weiss, R.; Rietjens, I. M. C. M. *J. Biol. Inorg. Chem.* **1999**, *4*, 274.
(96) Spee, J. H.; Boersma, M. G.; Veeger, C.; Samyn, B.; Van Beeumen, J.; Warmerdam, G.; Canters, G. W.; Van Dogen, W. M. A. M.; Rietjens, I. M. C. M. *Eur. J. Biochem.* **1996**, *241*, 215.
(97) Low, D. W.; Gray, H. B.; Duus, J. O. *J. Am. Chem. Soc.* **1997**, *119*, 1.
(98) Casella, L.; De Gioia, L.; Frontoso Silvestri, G.; Monzani, E.; Redaelli, C.; Roncone, R.; Santagostini, L. *J. Inorg. Biochem.* **2000**, *79*, 31.
(99) Mashino, T.; Nakamura, S.; Hirobe, M. *Tetrahedron Lett.* **1990**, *31*, 3163.
(100) Boersma, M. G.; Primus, J. L.; Koerts, J.; Veeger, C.; Rietjens, I. M. C. M. *Eur. J. Biochem.* **2000**, *267*, 6673.
(101) Ricoux, R.; Bouchler, J. L.; Mansuy, D.; Mahy, J. P. *Biochem. Biophys. Res. Commun.* **2000**, *278*, 217.
(102) Tatsuma, T.; Mori, H.; Fujishima, A. *Anal. Chem.* **2000**, *72*, 2919.
(103) Casella, L.; Gullotti, M.; De Gioia, L.; Monzani, E.; Chillemi, F. *J. Chem. Soc., Dalton Trans.* **1991**, 2945.
(104) Casella, L.; Gullotti, M.; De Gioia, L.; Bartesaghi, R.; Chillemi, F. *J. Chem. Soc., Dalton Trans.* **1993**, 2233.
(105) Casella, L.; Monzani, E.; Fantucci, P.; Gullotti, M.; De Gioia, L.; Strini, A.; Chillemi, F. *Inorg. Chem.* **1996**, *35*, 439.
(106) Monzani, E.; Linati, L.; Casella, L.; De Gioia, L.; Favretto, M.; Gullotti, M.; Chillemi, F. *Inorg. Chim. Acta* **1998**, *273*, 339.
(107) Franceschi, F.; Gullotti, M.; Monzani, E.; Casella, L.; Papaefthymiou, V. *Chem. Commun.* **1996**, 1645.
(108) Monzani, E.; Casella, L.; Gullotti, M.; Panigada, N.; Franceschi, F.; Papaefthymiou, V. *J. Mol. Catal.* **1997**, *117*, 199.
(109) Ferguson-Miller, S.; Babcock, G. T. *Chem. Rev.* **1996**, *96*, 2889.
(110) Nastri, F.; Lombardi, A.; Morelli, G.; Maglio, O.; D′Auria, G.; Pedone, C.; Pavone, V. *Chem. Eur. J.* **1997**, *3*, 340.
(111) D′Auria, G.; Maglio, O.; Nastri, F.; Lombardi, A.; Mazzeo, M.; Morelli, G.; Paolillo, L.; Pedone, C.; Pavone, V. *Chem. Eur. J.* **1997**, *3*, 350.
(112) Lombardi, A.; Nastri, F.; Sanseverino, M.; Maglio, O.; Pedone, C.; Pavone, V. *Inorg. Chim. Acta* **1998**, *275*−*276*, 301.
(113) Nastri, F.; Lombardi, A.; Morelli, G.; Pedone, C.; Pavone, V.; Chottard, G.; Battioni, P.; Mansuy, D. *J. Biol. Inorg. Chem.* **1998**, *3*, 671.
(114) D′Andrea, L. D.; Nastri, F.; Lombardi, A.; Maglio, O.; Pavone, V.; Miniaturized Hemoproteins: A Covalent Asymmetric Peptide-Porphyrin System. In *Peptides 98*; Bajusz, S., Hudecz, F., Eds.; Akadémia Kiadó: Budapest, Hungary, 1999; pp 304−305.
(115) Fermi, G.; Perutz, M. F.; Shaanan, B.; Fourme, R. *J. Mol. Biol.* **1984**, *175*, 159.
(116) Lombardi, A.; Summa, C.; Geremia, S.; Randaccio, L.; Pavone, V.; DeGrado, W. F. *Proc. Natl. Acad. Sci.* **2000**, *97*, 6298.
(117) Lombardi, A.; Marasco, D.; Maglio, O.; Di Costanzo, L.; Nastri, F.; Pavone, V. *Proc. Natl. Acad. Sci.* **2000**, *97*, 11922.
(118) Arnold, P. A.; Benson, D. R.; Brink, D. J.; Hendrich, M. P.; Jas, G. S.; Kennedy, M. L.; Petasis, D. T.; Wang, M. *Inorg. Chem.* **1997**, *36*, 5306.

(119) Wang, M.; Kennedy, M. L.; Hart, B. R.; Benson, D. R. *Chem. Commun.* **1997**, 883.
(120) Williamson, D. A.; Benson, D. R. *Chem. Commun.* **1998**, 961.
(121) Liu, D.; Williamson, D. A.; Kennedy, M. L.; Williams, T. D.; Morton, M. M.; Benson, D. R. *J. Am. Chem. Soc.* **1999**, *121*, 11798.
(122) Liu, D.; Lee, K.-H.; Benson, D. R.*Chem. Commun.* **1999**, 1205.
(123) Mihara, H.; Haruta, Y.; Sakamoto, S.; Nishino, N.; Aoyagi, H. *Chem. Lett.* **1996**, 1.
(124) Obataya, I.; Kotaki, T.; Sakamoto, S.; Ueno, A.; Mihara, H. *Bioorg. Med. Chem. Lett.* **2000**, *10*, 2719.
(125) Tuchscherer, G.; Mutter, M. *J. Biotechnol.* **1995**, *41*, 197.
(126) Schneider, J. P.; Kelly, J. W. *Chem. Rev.* **1995**, *95*, 2169.
(127) DeGrado, W. F.; Lear, J. D. *Biopolymers* **1990**, *29*, 205.
(128) Mihara, H.; Nishino, N.; Hasegawa, R.; Fujimoto, T. *Chem. Lett.* **1992**, 1805.
(129) Mihara, H.; Tomizaki, K.; Fujimoto, T.; Sakamoto, S.; Aoyagi, H.; Nishino, N. *Chem. Lett.* **1996**, 187.
(130) Henderson, R.; Baldwin, J. M.; Ceska, T. A.; Zemlin, F.; Beckmann, E.; Downing, K. H. *J. Mol. Biol.* **1990**, *213*, 899.
(131) Geier, G. R., III; Sasaki, T. *Tetrahedron Lett.* **1997**, *38*, 3821.
(132) Karpishin, T. B.; Vannelli, T. A.; Glover, K. J. *J. Am. Chem. Soc.* **1997**, *119*, 9063.
(133) Kamtekar, S.; Hecht, M. *FASEB J.* **1995**, *9*, 1013.
(134) Weber, P. C.; Bartsch, R. G.; Cusanovich, M. A.; Hamlin, R. C.; Howard, A.; Jordan, S. R.; Kamen, M. D.; Meyer, T. E.; Weatherford, D. W.; Xuong, N. G.; Salemme, F. R. *Nature* **1980**, *286*, 302.
(135) Xavier, A. V.; Czerwinski, E. W.; Bethge, P. H.; Mathews, F. S. *Nature* **1978**, *275*, 245.
(136) Lederer, F.; Glatigny, A.; Bethge, P. H.; Bellamy, H. D.; Mathews, F. S. *J. Mol. Biol.* **1981**, *148*, 427.
(137) Presnell, S. R.; Cohen, F. E. *Proc. Natl. Acad. Sci.* **1989**, *86*, 6592.
(138) Hill, R. B.; Raleigh, D. P.; Lombardi, A.; DeGrado, W. F. *Acc. Chem. Res.* **2000**, *33*, 745.
(139) Murzin, A. C.; Chothia, C. *Curr. Opin. Struct. Biol.* **1992**, *2*, 895.
(140) Rozwarski, D. A.; Gronenborn, A. M.; Clore, G. M.; Bazan, J. F.; Bohm, A.; Wlodawer, A.; Hatada, M.; Karplus, P. A. *Structure* **1994**, *2*, 159.
(141) Banner, D. W.; Kokkinidis, M.; Tsernoglou, D. *J. Mol. Biol.* **1987**, *196*, 657.
(142) Betz, S. F.; DeGrado, W. F. *Biochemistry* **1996**, *35*, 6955.
(143) Hill, R. B.; DeGrado, W. F. *J. Am. Chem. Soc.* **1998**, *120*, 1138.
(144) Betz, S. F.; Liebman, P. A.; DeGrado, W. F. *Biochemistry* **1997**, *36*, 2450
(145) Kohn, W. D.; Mant, C. T.; Hodges, R. S. *J. Biol. Chem.* **1997**, *272*, 2583.
(146) Nagi, A. D.; Regan, L. *Folding Des.* **1996**, *2*, 67.
(147) Brive, L.; Dolphin, G. T.; Baltzer, L. *J. Am. Chem. Soc.* **1997**, *119*, 8598.
(148) Starovasnik, M. A.; Braisted, A. C.; Wells, J. A. *Proc. Natl. Acad. Sci. U.S.A.* **1997**, *94*, 10080.
(149) Braisted, A. C.; Wells, J. A. *Proc. Natl. Acad. Sci. U.S.A.* **1996**, *93*, 5688.
(150) Cunningham, B. C.; Wells J. A. *Curr. Opin. Struct. Biol.* **1997**, *7*, 457.
(151) Munson, M.; Balasubramanian, S.; Fleming, K. G., Nagi, A. D.; O'Brien, R.; Sturtevant, J. M.; Regan, L. *Protein Sci.* **1996,** *5*, 1584.
(152) Kamtekar, S.; Schiffer, J. M.; Xiong, H.; Babik, J. M.; Hecht, M. H. *Science* **1993,** *262*, 1680.
(153) Roy, S.; Ratnaswamy, G.; Boice, J. A.; Fairman, R.; McLendon, G.; Hecht, M. H. *J. Am. Chem. Soc.* **1997**, *119*, 5302.
(154) Rojas, N. R. L.; Kamtekar, S.; Simons, C. T.; McLean, J. E.; Vogel, K. M.; Spiro, T. G.; Farid, R. S.; Hecht, M. H. *Protein Sci.* **1997**, *6*, 2512.
(155) Roy, S.; Hecht, M. H. *Biochemistry* **2000**, *39*, 4603.
(156) Sakamoto, S.; Sakurai, S.; Ueno, A.; Mihara, H. *Chem. Commun.* **1997**, 1221.
(157) Sakamoto, S.; Ueno, A.; Mihara, H. *Chem. Commun.* **1998**, 1073.
(158) Sakamoto, S.; Ueno, A.; Mihara, H. *J. Chem. Soc., Perkin Trans. 2* **1998**, 2395.
(159) Sakamoto, S.; Obataya, I.; Ueno, A.; Mihara, H. *J. Chem. Soc., Perkin Trans. 2* **1999**, 2059.
(160) Sakamoto, S.; Obataya, I.; Ueno, A.; Mihara, H. *Chem. Commun.* **1999**, 1111.
(161) Obataya, I.; Sakamoto, S.; Ueno, A.; Mihara, H. *Protein Pept. Lett.* **1999**, *6*, 141.
(162) Takahashi, M.; Ueno, A.; Uda, T.; Mihara H. *Biorg. Med. Chem. Lett.* **1998**, *8*, 2023.
(163) Takahashi, M.; Ueno, A.; Mihara, H. *Chem. Eur. J.* **2000**, *6*, 3196.
(164) McLachlan, A. D.; Stewart, M. *J. Mol. Biol.* **1975**, *98*, 293.
(165) Huffman, D. L.; Rosenblatt, M. M.; Suslick, K. S. *J. Am. Chem. Soc.* **1998**, *120*, 6183.
(166) Arnold, P. A.; Shelton, W. R.; Benson, D. R. *J. Am. Chem. Soc.* **1997**, *119*, 3183.
(167) Choma, C. T.; Lear, J. D.; Nelson, M. J.; Dutton, P. L.; Robertson, D. E.; DeGrado, W. F. *J. Am. Chem. Soc.* **1994**, *116*, 856.
(168) Robertson, D. E.; Farid, R. S.; Moser, C. C.; Urbauer, J. L.; Mulholland, S. E.; Pidikiti, R.; Lear, J. D.; Wand, A. J.; DeGrado, W. F.; Dutton, P. L. *Nature* **1994**, *368*, 425.
(169) Kalsbeck, W. A.; Robertson, D. E.; Pandey, R. K.; Smith, K. M.; Dutton, P. L.; Bocian, D. F. *Biochemistry* **1996**, *35*, 3429
(170) Shifman, J. M.; Gibney, B. R.; Sharp, R. E.; Dutton, P. L. *Biochemistry* **2000**, *39*, 14813.
(171) Shifman, J. M.; Moser, C. C., Kalsbeck, W. A., Bocian, D. F., Dutton, P. L. *Biochemistry* **1998**, *37*, 16815.
(172) Gibney, B. R.; Isogay, Y.; Rabanal, F.; Reddy, K. S.; Grosset, A. M.; Moser, C. C.; Dutton, P. L. *Biochemistry* **2000**, *39*, 11041.
(173) Gibney, B. R.; Dutton, P. L. *Protein Sci.* **1999**, *8*, 1888.
(174) Rabanal, F.; DeGrado, W. F.; Dutton, P. L. *J. Am. Chem. Soc.* **1996**, *118*, 473.
(175) Gibney, B. R.; Rabanal, F.; Skalicky, J. L.; Wand, A. L.; Dutton, P. L. *J Am. Chem. Soc.* **1997**, *119*, 2323.
(176) Skalicky, J. J.; Gibney, B. R.; Rabanal, F.; Bieber-Urbauer, R. J.; Dutton, P. L.; Wand, A. J. *J. Am. Chem. Soc.* **1999**, *121*, 4941.
(177) Gibney, B. R.; Rabanal, F.; Reddy, K. S.; Dutton, P. L. *Biochemistry* **1998**, *37*, 4635.
(178) Gibney, B. R.; Johansson, J. S.; Rabanal, F.; Skalicky, J. J.; Wand, A. J.; Dutton, P. L. *Biochemistry* **1997**, *36*, 2798.
(179) Gibney, B. R.; Mulholland, S. E., Rabanal, F.; Dutton, P. L. *Proc. Natl. Acad. Sci.* **1996**, *93*, 15041.
(180) Sharp, R. E.; Moser, C. C.; Rabanal, F.; Dutton, P. L. *Proc. Natl. Acad. Sci.* **1998**, *95*, 10465.
(181) Sharp, R. E.; Diers, J. R.; Bocian, F.; Dutton, P. L. *J. Am. Chem. Soc.* **1998**, *120*, 7103.
(182) Gibney, B. R.; Rabanal, F.; Skalicky, J. J.; Wand, A. J.; Dutton, P. L. *Biochemistry* **1999**, *121*, 4952.
(183) Ho, S. P.; DeGrado, W. F. *J. Am. Chem. Soc.* **1987**, *109*, 6751.
(184) Yun, C. H.; Crofts, A. R.; Gennis, R. B. *Biochemistry* **1991,** *30*, 6747.
(185) Xia, D.; Yu, C. A.; Kim, H.; Xia, J. Z.; Kachurin, A. M.; Zhang, L.; Yu, L.; Deisenhofer, J. *Science* **1997**, *277*, 60.
(186) Rau, H. K.; Haehnel, W. *J. Am. Chem. Soc.* **1998**, *120*, 468.
(187) Rau, H. K.; DeJonge, N.; Haehnel, W. *Proc. Natl. Acad. Sci.* **1998**, *95*, 11526.
(188) Kramer, D. M.; Crofts, A. R. *Biochim. Biophys. Acta* **1994**, *1184*, 193.
(189) Rau, H. K.; DeJonge, N.; Haehnel, W. *Angew. Chem., Int. Ed.* **2000**, *39*, 250.
(190) Moffet, D. A.; Certain, L. K.; Smith, A. J.; Kessel, A. J.; Beckwith, K. A.; Hecht, M. H. *J. Am. Chem. Soc.* **2000**, *122*, 7612.
(191) Moffet, D. A.; Case, M. A.; House, J. C.; Vogel, K.; Williams, R. D.; Spiro, T. G.; McLendon, G. L.; Hecht, M. H. *J. Am. Chem. Soc.* **2001**, *123*, 2109.
(192) Springer, B. A.; Sligar, S. G.; Olson, J. S.; Phillips, G. N., Jr. *Chem. Rev.* **1994**, *94*, 699.
(193) Sakamoto, M.; Ueno, A.; Mihara, H. *Chem. Commun.* **2000**, 1741.
(194) Sakamoto, M.; Ueno, A.; Mihara, H. *Chem. Eur. J.* **2001**, in press.

CR000055J